M. Kamphus, M. Braun-Unkhoff., K. Kohse-Höinghaus, Formation of small PAHs in laminar premixed low-pressure propene and cyclopentene flames: Experiment and modeling, Combust. Flame 152 (2008) 28–59.

The original publication is available at www.elsevier.com

http://dx.doi.org/10.1016/j.combustflame.2007.09.005

Formation of small PAHs in laminar premixed low-pressure propene and cyclopentene flames: Experiment and modelling

M. Kamphus[1], M. Braun-Unkhoff[2], K. Kohse-Höinghaus[1]
[1] *Physikalische Chemie I, Universität Bielefeld, Germany*
[2] *Deutsches Zentrum für Luft- und Raumfahrt e.V., Stuttgart, Germany*

Abstract
The formation of small PAHs with up to three rings has been studied in fuel-rich, nonsooting premixed flames of propene–oxygen–argon and cyclopentene–oxygen–argon at C/O = 0.77 and 50 mbar. Detailed species composition and temperature profiles for these flames had been studied before, using laser-induced fluorescence (LIF) and in situ molecular beam mass spectrometry (MBMS) with electron impact ionization (EI). These previous studies found a significant influence of the fuel structure upon the reaction pathways to benzene as the first aromatic ring. Here, the further molecular reaction sequence is studied with enhanced sensitivity, using MBMS coupled with resonance-enhanced multiphoton ionization (REMPI). Absolute concentrations of benzene were determined using both ionization strategies in order to establish a link to the previous investigations. The ratio of REMPI signals in the two flames for masses from *m/z* = 78 (benzene) up to approximately *m/z* = 200 is given and shows a predominant tendency of the cyclopentene flame to form aromatic species. The experimental results are complemented with simulations using two current chemical kinetic reaction models. The model predictions for important species in this mass range are discussed in the light of reaction flux and sensitivity analyses.

Keywords: PAH formation; Premixed flames; Propene; Cyclopentene; In situ mass spectrometry; Detailed chemical kinetic modeling

Introduction

Aromatic species and polycyclic aromatic hydrocarbons (PAHs) are formed in the combustion of many hydrocarbons and their emission is of particular concern because of their potentially adverse health effects. They may originate from waste incineration or from the combustion of practical fuels such as kerosene, and they are emitted in significant amounts by vehicles and airplanes. Aromatics may be important constituents of the fuel itself. For example, gasoline consists of up to 32% aromatics [1], and kerosene is a complex mixture of alkanes, mono- and polycyclic aromatics, and cycloalkanes or naphthenes [2]. Furthermore, aromatic species have been identified as key precursors of soot, where large carbonaceous structures are built up from fuel molecules and small intermediates with much lower numbers of carbon atoms. PAHs play a decisive role in this mechanism, and particle inception is described in nearly all current soot models exclusively by coagulation of large-mass PAHs [3]. The

assembly of the first aromatic ring, benzene (A1, C_6H_6), from its precursor molecules is commonly considered as the first step toward PAH formation and growth [4–6].

Pathways to further small aromatic structures from fuels of different molecular structure remain a subject of intense study and discussion [4–15]. For the simulation of particle inception, it may suffice under some conditions to consider only a few PAH species that appear in high concentrations [7]. The importance of PAH submodels for soot particle inception and soot yield, however, has been discussed in several studies [3,9,14] relying on shock tube experiments and flame investigations, in particular at high pressures. Here, the initial molecular stages of PAH growth are regarded as particularly interesting in view of the different structures of small aromatic compounds as building blocks or templates for further growth.

Modeling the complete soot formation process is still a challenging task. Current soot models combine comprehensive gas-phase reaction mechanisms for the description of fuel breakup, formation, and growth of PAHs, with a submodel to predict soot particle inception, growth, and oxidation. The chemical kinetic gas-phase mechanism typically takes about a hundred or more species and several hundred reactions into account [8,16–20]. Such molecular gas-phase mechanisms are capable of predicting the concentrations of stable and reactive intermediates for molecules up to benzene and indene in premixed low-pressure flames with acceptable accuracy [8,16–18]. However, the influence of the fuel structure itself on the molecular reaction mechanisms beyond benzene has not been studied in detail, and quantitative experimental data for validation and model optimization are largely lacking. Of special interest seems the growth of PAHs with two to five fused or loosely connected C_5- and C_6-rings with and without aliphatic side chains [6,17, 18], since the transition from the molecular chemical kinetic mechanism to the soot submodel is currently considered at molecular sizes of four or five aromatic rings. In this transition region, a highly accurate picture of the gas-phase species composition would be desirable, since the reactive species mix in this regime is of paramount influence on the further growth process.

In summary, mechanistic understanding and a reliable description of the formation of small aromatic structures are of fundamental interest and critical for meaningful soot modeling with the aim of reducing respective emissions from combustion processes. Therefore, the investigation of PAH formation routes in laboratory flames of exemplary fuels with different chemical structures seems warranted to gain more detailed insight into this problem.

Sampling techniques have made it possible to gain important knowledge on the concentrations of small PAHs in laboratory flames of a broad variety of fuels [15,21]. Molecular beam mass spectrometry (MBMS) is established as one of the most common techniques for investigating benzene and PAH formation in laminar premixed low-pressure flames. Previous measurements with MBMS in low pressure flames have typically characterized molecules up to naphthalene quantitatively with direct calibration [17,22] and molecules up to the $C_{20}H_x$– $C_{48}H_x$ range and fullerenes up to C_{84} qualitatively, using a sublimation technique [23]. One of the challenges in measuring quantitative concentration profiles of these intermediates of larger aromatic species is their low vapor pressure, and calibration mixtures with known concentrations are already not easily provided for species featuring two or three aromatic rings. For example, the maximum concentration of naphthalene that can be supplied in a typical calibration gas mixture at room temperature is about 10 ppm. Also, the typical sensitivity of electron impact ionization (EI)-MBMS at low ionization energies of 11–13 eV, which limit fragmentation, is 10^{-5}, often too low for quantitative detection of small PAHs.

For these reasons, the present study reports a mass spectrometric investigation of laminar premixed lowpressure flames of propene and cyclopentene, both with a C/O ratio of 0.77, in the mass region beyond *m/z* = 78 (benzene) to *m/z* = 202 (pyrene, fluoranthene). Both flames are fuel-rich, but not sooting. They have been studied before using laser-induced fluorescence (LIF) thermometry and EI-MBMS to provide stable and reactive intermediate species concentrations up to benzene [17,24–27]. In addition, recent investigations have studied both the cyclopentene flame [28] and the propene flame [29] again, using tunable vacuum UV (VUV) light as a photoionization (PI) source in MBMS measurements to identify key intermediate species. The chemistry of the propene flame has already been modeled by several groups [11,13,17], and the cyclopentene flame was modeled by Lindstedt and Rizos [16]. From these studies, the pathways to benzene have been shown to exhibit substantial differences in these two flames [30], with the predominant benzene-forming reactions being propargyl recombination and further reactions involving C_3-radicals in the propene flame and contributions of C_5-reactions such as that of cyclopentadienyl with methyl [31,32] in the cyclopentene flame. The individual importance of these and other benzene-forming reactions has been discussed [30] in light of their temperature-dependent reaction coefficients, which remain partly under discussion. It has not been attempted before to our knowledge to simulate these different chemistries with the same mechanism.

In this paper, we have employed resonance-enhanced multiphoton ionization (REMPI)-MBMS to enhance the sensitivity toward larger aromatic species and to provide ratios of their concentrations. The benzene concentration profile has been measured in both flames using both ionization strategies, i.e., EI- and REMPI-MBMS, to provide a link between these and previous measurements [24,25,30].

Detailed modeling of the species composition in both flames is used to study the different flame chemistries. For this, two fuel-rich gas-phase mechanisms have been adapted and employed, together with reaction flow and sensitivity analyses, to gain insight into small PAH formation pathways and to provide clues for further study and optimization.

2. Experiment

Two premixed, laminar, flat flames at 50 mbar were investigated, which burnt on a temperaturestabilized (water flow of T = 313 K) sintered bronze plate of diameter 62.8 mm: a propene–oxygen–argon flame (cold gas flows 1.111, 2.155, and 1.089 slm, respectively) and a cyclopentene–oxygen–argon flame (cold gas flows 0.725, 2.345, and 1.023 slm, respectively). Both flames had a C/O ratio of nominally 0.77. Gas flows were controlled by calibrated mass flow controllers (Tylan Series 2900), with the exception of that of cyclopentene. Cyclopentene (b.p. 317 K) stabilized with 0.01% 2,6-di-*tert*-butyl-*p*cresol was electrically heated to 310 K, and its gas flow to the burner was controlled by a microvalve and calibrated by differential weighting. All tubes to the burner were heated to 313 K. These flames had been studied previously using EI-MBMS, and some of the reported species profiles are also compared with the model calculations in the present investigation; details about procedures and calibration can be found in [17, 24,27] for the propene flame and in [25] for the cyclopentene flame. Typically, error limits are estimated to be within a factor of 3 for radical intermediate species for which direct calibration was not possible [17,24,25,27]. Further investigations of these flames as part of a study of the combustion chemistry of C_5-fuels [30] are generally in satisfactory agreement. The benzene profile was determined in the present paper with both EI-MBMS and REMPI-MBMS, using a certified test gas mixture. The measurements are in reasonable accord with recent studies using VUVPI- MBMS [28,29]. Calibration in that case relies on photoionization rather than electron ionization cross sections, with a typical error factor of 2–4 when cross sections had to be estimated [28].

The analysis of the two flames in this work was performed with a time-of-flight mass spectrometer equipped with a gridless reflectron. The flame was probed with a quartz nozzle with an opening diameter of 120 μm and gas samples were expanded to 10^{-4} mbar. A second expansion through a copper skimmer with a diameter of 1.7 mm reduced the pressure to 10^{-6} mbar. In the molecular beam, the molecules were ionized with a Nd:YAG (Quantel Brilliant B) pumped dye laser (Lambda Physik Scanmate 2E) at 255 nm, using C307 as the dye. The ionization laser beam was unfocused, with laser intensities of ≤1 mJ/pulse and a pulse length of 5 ns.

An ionization wavelength of 255 nm was chosen to enable simultaneous detection of different aromatic compounds; Fig. 1 shows the respective absorption spectra. Alternatively, if radiation at 259 nm is used, corresponding to the $^1B_{2u} \leftarrow ^1A_{1g}\ 6^1_0$ transition of benzene, or near 210 nm, corresponding to the $^1B_{2u} \leftarrow ^1A_{1g}$ transition of naphthalene, the spectrum can be chosen to reflect predominantly the mass signal of benzene or those of naphthalene and methylnaphthalene, respectively.

Mass spectra were averaged over 200 laser pulses with a digital oscilloscope (LeCroy, A9350). Signals were collected in a time-of-flight region of 30–50 μs with a time resolution of 2 ns, resulting in a mass region of m/z = 50 to m/z = 210. Simultaneously, the laser intensity was measured with a home-built photodiode, amplified (SRS, SR240) and averaged with a boxcar-A/D-converter set-up (SRS, SR250 and SR245). The mass signals were analyzed after baseline correction and fitted with Gaussian functions.

For comparison of the two different flames, all important experimental parameters, especially for the mass spectrometer and ionization setup, were held constant. We thus assume that - to a first approximation - the ratio of a particular mass signal in the cyclopentene flame to that of the same mass in the propene flame is equivalent to the concentration ratio in these flames. This assumption is not appropriate if the signal at a particular mass is composed of contributions from different isomers (or different isomer mole fractions) in the two flames. Indications for such behavior will, however, be evident in comparison with modeling the two flames.

3. Modeling

The concentration profiles as a function of height above the burner surface were calculated for the two flames using the one-dimensional PREMIX code of the CHEMKIN package [33], with thermal diffusion. As input parameters, the measured temperature profiles, the mass flow rates and molar fractions of the reactants, and the burner's diameter were used. Thermodynamic data were taken from [34], whenever possible, and from the CHEMKIN thermodynamic database [35]. Transport properties were obtained from the SANDIA transport database [36] or as detailed in [20]. Transport properties for species not found in the database were estimated by applying analogy rules based on known species.

All calculations were performed with two different detailed reaction mechanisms: the DLR reaction mechanism and the MIT reaction mechanism of Richter and Howard [37]. Choosing two mechanisms rather than only one may be surprising, since modeling is sometimes performed to improve agreement between experimental data and one specific reaction model, potentially changing reaction sequences

and kinetic expressions. Our intention here is different. Regarding the complexity of the chemistry in fuel-rich combustion, we have attempted to use two established mechanisms, which have been continuously developed and validated against an appreciable number of different combustion situations, with the aim of identifying current limitations in the prediction of concentrations of small aromatic species. Both mechanisms were used as published, without modifications other than those explicitly stated in this paper. The DLR mechanism has been developed preferentially for ambient and higher pressures, and some rate expressions have been adapted to 50 mbar as reported, regarding their pressure dependence. The MIT model has been developed to model premixed low-pressure flames.

3.1. The DLR reaction mechanism

The DLR comprehensive gas-phase reaction mechanism, which enables the description of fuel-rich combustion processes including soot, has been developed over the past decade. The initial mechanism used successfully for the description of benzene oxidation [38] has been further improved. It was extended by including kinetic data from several studies [8,9,18–20]. In particular, results from shock tube experiments devoted to the investigation of elementary reactions of small aromatics and their precursors such as cyclopentadiene and cyclopentadienyl [39], toluene [40], phenol [41], and phenylacetylene [42] have been taken into account, including the reactions of radicals associated with these compounds, as well as those of the propargyl radical [43]—additions that have proven useful already in previous work at high pressure [7–9]. In particular, the branching ratio of reactions with aromatic species turned out to be important for the formation of soot precursors. For example, the recombination of propargyl radicals leads—at elevated temperatures—predominantly to the formation of benzene and not of phenyl and H-atoms [43]; furthermore, propargyl radicals can react with benzyl, which is produced by pyrolysis of benzene, leading to naphthalene (e.g., [44]).

This detailed gas-phase reaction mechanism was combined with a mechanistic soot model [3] that was modified [8] with respect to the growth and coagulation of PAHs and the formation of the first soot particles. The updated and refined PAH growth submodel contains about 96 species up to benzo[a,e]pyrene ($C_{20}H_{12}$) and 280 elementary reaction steps [9,14]. Dominant pathways include (i) the hydrogen abstraction carbon addition (HACA) or C_2-species addition reactions, (ii) the combinative growth path, which describes reactions between small aliphatic hydrocarbon radicals and aromatic species and results in faster PAH formation compared to the classical HACA sequence, and (iii) reactions of the cyclopentadienyl radical, such as the recombination reaction that produces naphthalene, and additional routes to form indene, which then can grow by further reactions with cyclopentadienyl. It should be noted, however, that the experimental database for the rate coefficients in the PAH mechanism is extremely poor. Therefore, most of the kinetic data had to be estimated from the comparison with similar reactions of smaller aromatics, as for example, splitting of a methyl group

by breaking a C–C bond after H-atom attack on a methylated PAH. Also, the thermodynamic data of the PAH species—which were taken from [13]—are of significant importance for the calculation of thermochemical equilibrium and reverse rate constants, respectively. However, some thermodynamic data for these large molecules are not available and must be calculated by quantum mechanical methods, which sometimes leads to relatively large errors.

The DLR mechanism has been applied to a large range of experimental systems, including shock tube pyrolysis and premixed flames [7–9,14,45–48]. Its C_1- to C_4-submodel was validated by modeling the concentration profiles measured in laminar, sooting ethane–oxygen–argon flames operated at atmospheric pressure [47]. In particular, the mechanism reproduces the experimental values for the C_1- and C_2- species concentrations very well. PAH formation in different sooting methane, ethane, ethylene and benzene flames was assessed [47]. In summary, good agreement was found when experimental profiles of reactants, intermediates including radicals, main products, small hydrocarbons, and light PAHs, as well as soot volume fraction, were modeled for a variety of parameters such as fuel, mixing ratio, temperature, and pressure for both laminar premixed flames and shock tube experiments.

To enable modeling of cyclopentene combustion, a submodel of 11 relevant reactions of $c\mathrm{C_5H_8}$- and $c\mathrm{C_5H_7}$-species was added, parameters for which are given in Table 1. This submodel was previously used in a modeling study of the oxidation of cyclohexane mixtures including laminar flame speed at atmospheric and high pressures [49]. Currently, the DLR reaction mechanism consists of 174 chemical species and 672 elementary reactions. Most of the gas-phase reactions are treated as reversible, with rate coefficients for the reverse reactions evaluated from the respective equilibrium constants. Only a few reaction steps, representing preferentially isomerization reactions, are considered with separate rate coefficient expressions for the forward and reverse directions.

3.2. The MIT reaction mechanism

This detailed chemical reaction mechanism in the version used here comprised 157 chemical species and 872 elementary reactions. It was designed for modeling of acetylene, ethylene, and benzene combustion in laminar premixed low-pressure flames. The mechanism has been applied successfully to rich acetylene, ethylene, and benzene flames as well as to a lean ethylene flame [50] and to a stoichiometric methane flame [51]. The formation of PAHs containing up to three condensed rings is included. The MIT reaction mechanism can be downloaded [37] and is discussed in [52]. For modeling the cyclopentene flame, the reaction sequence in Table 1 was added as for the DLR mechanism.

4. Results and discussion

In the following section, a comparison between predicted and measured experimental data is given for both flames, with emphasis on major species and on benzene; furthermore, the behavior of larger PAHs is discussed. The experimental data comprise three categories of results. First, major species, important intermediates, and some radical concentrations have been measured quantitatively with EI-MBMS before [17,24,25,27] as a function of height above the burner (HAB). These data are considered here as a basis for the simulation with both reaction models, in particular since some previous modeling results for these flames are available in the literature [11, 13,16,17]. Second, the benzene profile vs HAB was measured with both EI-MBMS and REMPI-MBMS in the present study. In this case, quantitative predictions with both models will emphasize and com pare important features of early ring formation chemistry. Third, for aromatic species beyond benzene, relative concentration profiles were obtained here by REMPI-MBMS, for which absolute calibration measurements were not feasible. However, species profiles and their maximum signal intensities were measured in both flames for a variety of species up to about m/z = 200, and the ratios of these maximum signal intensities, $I_{\text{cyclopentene}}/I_{\text{propene}}$, obtained under identical conditions, are assumed to reflect the respective concentration ratios. The experimental results are not isomer-specific, while both models may include several chemical structures for a given mass. For a detailed comparison of the measured intensity (concentration) ratios with model predictions, this issue must be taken into account by appropriate addition of simulated species concentrations for the different mass isomers. Reaction flux and sensitivity analyses are carried out to identify main PAH growth routes and to determine important reactions of selected species. Note that—to enable direct comparison with the two reaction mechanisms and elementary steps given therein—we use their respective nomenclature for species; thus, species may have different short representations (such as A1 for benzene in the DLR model and C_6H_6 in the MIT reaction mechanism, respectively) in the two mechanisms, which are not always consistent with IUPAC rules.

4.1. Reactants and major products

Measured and predicted species profiles of reactants and major products, as well as temperature profiles measured by optical techniques within an accuracy of typically 100 K in the burnt gas [26], are displayed in Fig. 2 for the propene flame and in Fig. 3 for the cyclopentene flame. Note that the maximum temperature and the temperature in the burnout zone are about 100 K higher for the propene flame; also, the reaction zones are located at different heights, ~5–6 mm in the propene flame and ~3 mm in the cyclopentene flame.

The mole fractions of reactants—namely propene, cyclopentene, and oxygen—and of the inert additive argon are reproduced well concerning shape and absolute values, as shown in the top frames of Figs. 2 and 3. In particular, the depletion of fuel and oxygen is well predicted by both reaction models. Close to the burner surface, the predicted initial concentrations of the reactants are lower than those of the measured ones. This behavior is caused by the high thermal diffusion of hydrogen, leading to considerably higher calculated H_2 profiles than observed. This is especially pronounced for the cyclopentene flame (Fig. 3), where a similar effect has already been noted earlier [16] and discussed in view of different temperature profiles in the preheat zone. Concerning the other major products—carbon monoxide, carbon dioxide, and water—the comparison between experimental and calculated species profiles reveals an overestimation of CO_2 for both flames. For the propene flame (Fig. 2), CO is slightly overpredicted at lower HAB, but matched in the burnout zone, whereas the calculated H_2O mole fraction is lower than the measured one. For the cyclopentene flame (Fig. 3), experimental mole fractions of CO are matched at lower HAB, but underpredicted in the burnt gas, whereas the mole fraction of H_2O is overpredicted considerably for all measured heights, despite the relatively wide uncertainty range. It should be noted, however, that the shapes of all major species concentration profiles are matched well by the model predictions. Simulations with the DLR mechanism show a slightly better overall agreement than with the MIT mechanism. Also, the temperature sensitivity of the results was exemplarily tested by reducing the temperature in the propene flame by about 200 K to reflect potential cooling of the flame by the sampling nozzle. The general behavior of the major species mole fractions upon this temperature variation is quite robust, with only moderate changes in the different profiles, the most important ones noted in the H_2 concentrations. In the DLR mechanism, a reaction flux analysis identifies the main consumption pathways for the fuel propene as follows: (i) thermal decomposition and H-abstraction leading to the formation of propenyl (C_3H_5) radicals (R12, R14) and to the formation of methyl (CH_3) and vinyl (C_2H_3) radicals (R13); (ii) thermal decomposition of propenyl leading to propyne (pC_3H_4, R15) and allene (aC_3H_4, R16); (iii) propyne and allene reactions leading mainly to propargyl radicals (C_3H_3; R17–R22); and (iv) propargyl recombination to benzene (A1, R23), besides its H-abstraction leading to the C_3H_2 radical (R25). The C_3H_2 radical will then lead via the intermediates HCCO and HCO to the major products CO and CO_2. Thus, the formation sequence for PAH growth is initiated:

$$C_3H_6 \rightarrow C_3H_5 + H, \quad \text{(R12)}$$

$$C_3H_6 \rightarrow C_2H_3 + CH_3, \quad \text{(R13)}$$

$$C_3H_6 + H \rightarrow C_3H_5 + H_2, \quad \text{(R14)}$$

$$C_3H_5 \rightarrow pC_3H_4 + H, \quad \text{(R15)}$$

$$C_3H_5 \rightarrow aC_3H_4 + H, \quad \text{(R16)}$$

$$pC_3H_4 \rightarrow C_3H_3 + H, \quad \text{(R17)}$$

$a\mathrm{C_3H_4} \rightarrow \mathrm{C_3H_3} + \mathrm{H}$, (R18)

$p\mathrm{C_3H_4} + \mathrm{H} \rightarrow \mathrm{C_2H_2} + \mathrm{CH_3}$, (R19)

$p\mathrm{C_3H_4} + \mathrm{H} \rightarrow \mathrm{C_3H_3} + \mathrm{H_2}$, (R20)

$p\mathrm{C_3H_4} + \mathrm{OH} \rightarrow \mathrm{C_3H_3} + \mathrm{H_2O}$, (R21)

$a\mathrm{C_3H_4} + \mathrm{OH} \rightarrow \mathrm{C_3H_3} + \mathrm{H_2O}$, (R22)

$2\mathrm{C_3H_3} \rightarrow \mathrm{A1}$, (R23)

$\mathrm{C_3H_3} + \mathrm{H} \rightarrow \mathrm{C_3H_2} + {}_{\mathrm{H}}2$. (R25)

Concerning the cyclopentene flame, the fuel itself is mainly consumed via (i) its thermal decay leading to cyclopentadiene ($c\mathrm{C_5H_6}$, R1), which (ii) undergoes thermal decomposition and H-abstraction forming cyclopentadienyl ($c\mathrm{C_5H_5}$, R57, R58); this (iii) will react very fast to propargyl radicals via an isomerization step (R59, R60) and (iv) propargyl radicals will produce benzene (R23), thus initiating PAH growth:

$c\mathrm{C_5H_8} \rightarrow c\mathrm{C_5H_6} + \mathrm{H_2}$, (R1)

$c\mathrm{C_5H_6} \rightarrow c\mathrm{C_5H_5} + \mathrm{H}$, (R57)

$c\mathrm{C_5H_6} + \mathrm{H} \rightarrow c\mathrm{C_5H_5} + \mathrm{H_2}$, (R58)

$c\mathrm{C_5H_5} \rightarrow I\text{-}\mathrm{C_5H_5}$, (R59)

$I\text{-}\mathrm{C_5H_5} \rightarrow \mathrm{C_3H_3} + \mathrm{C_2H_2}$, (R60)

$2\mathrm{C_3H_3} \rightarrow \mathrm{A1}$. (R23)

It should be noted here that the only reactions that will be discussed explicitly in this paper are identified by a given number (R*n*)—not necessarily identical with that in any of the published mechanisms—while the respective reverse reaction is assigned a minus sign (R−*n*). Numbers are assigned consecutively, addressing the decomposition of the respective fuel first, and then increasing approximately with the buildup of larger molecular species.

The analysis shows that major species concentrations are—in general—satisfactorily reproduced by both models used here. Quite promising agreement and similar tendencies were also noted in [17] for the propene flame, where the initial discrepancy for oxygen is linked to the overestimated initial hydrogen concentration. Also, the mole fractions of $\mathrm{H_2}$, CO, $\mathrm{CO_2}$, and $\mathrm{H_2O}$ are matched within experimental error by the model of Hoyermann et al. [13], with the most substantial discrepancy (up to 30%) again seen in the hydrogen profile. For the cyclopentene flame, the overall structure is also reasonably well reproduced by the model developed by Lindstedt and Rizos [16], who noted some deviations from the experiment in the preheat zone. The temperature profiles used in the models were

modified within the experimental uncertainty (50–200 K variation) here, as well as in [13,17], for the propene flame, and in [16] for the cyclopentene flame. Tendencies are quite similar to those in this work, and we conclude that previous and present modeling attempts predict the general flame structure reasonably well for both fuels. The fuel decomposition pathways are quite different, as detailed above, and the radical pool must be analyzed in detail for both flames to predict the importance of specific pathways for the assembly of small ring compounds.

4.2. Intermediates and lighter hydrocarbons

Methyl (CH_3) and propargyl radicals (C_3H_3 in the DLR, H_2CCCH in the MIT model) are known to play an important role in the formation of aromatic species (see, e.g., [17,53]). Computed profiles for both species are shown in Fig. 4, together with experimental results, as a function of height above burner for both investigated flames. The profiles are characterized by sharp maxima. In the propene flame, the maxima are predicted at lower HAB than found in the experiment, whereas for the cyclopentene flame, the predicted maxima are shifted to slightly higher HAB. Both reaction models lead to very similar methyl profiles. Regarding the absolute mole fractions, the overall agreement for these two radical species is quite good, although it is somewhat less satisfactory with respect to the shape of the profiles. For the propene flame, methyl and propargyl are underestimated by less than a factor of 2, and for the cyclopentene flame, methyl is well predicted by both models, while propargyl is overpredicted by a factor of 4 (DLR model) or 7 (MIT model).

Two important stable C_2-hydrocarbon intermediates, acetylene (C_2H_2) and ethene (C_2H_4), are represented in Fig. 5. Acetylene in particular plays a dominant role in the formation and growth of PAHs via the HACA sequence. The shapes of the experimental profiles are reasonably well matched by the calculations. Acetylene persists toward the burnt gases—a fact that is also seen in the models. The simulated ethene profiles are somewhat broader than the measured ones. While experimental ethene and acetylene mole fractions are similar, both mechanisms predict higher acetylene than ethene concentrations for both flames. For the propene flame, the two models deviate considerably from each other, while predictions are similar for the cyclopentene flame. In the latter, both models overpredict the acetylene concentration by about a factor of 3 and underpredict the ethene concentration by more than a factor of 5. Earlier modeling studies (with different kinetic mechanisms) show quite good agreement for both species in the propene flame [13,17]. Recent VUV-PI-MBMS measurements of these species in the cyclopentene flame [28] reproduce our earlier EI-MBMS experiments within a factor of 3, and good agreement with the model predictions in the present study is noted. It should be remembered, however, that a consistent mechanism has not yet been used to predict the detailed structure of both flames.

Important representatives of stable C_4-compounds are diacetylene, C_4H_2, and vinylacetylene, C_4H_4. These species are of some interest with regard to the formation of higher-order stable and radical hydrocarbons and aromatics. Some features of the observed species profiles are matched by the models, as shown in Fig. 6. For example, vinylacetylene is consumed nearly totally in both flames, as in the experiment. Similarly, measured diacetylene mole fractions decay completely toward the burnt gas, whereas both models predict that noticeable concentrations of diacetylene remain in the post flame. The sequence of the maxima, with vinylacetylene being formed earlier than diacetylene, is consistent in the experiment and both models. Regarding the predictions with the DLR model, in the propene flame, more diacetylene is formed at lesser heights and at higher concentrations than vinylacetylene, whereas in the cyclopentene flame, vinylacetylene is produced earlier. This finding is consistent with the measurements, and experimental and calculated concentration maxima agree within a factor of 2–3. Earlier comparisons of measured C_4-species profiles in the propene flame with different models [13,17] have also reported underestimation of the experimental values (note the better agreement of peak positions, which is in part due to shifting the experimental profiles [13,17]). The influence of C_4-species on benzene formation was discussed as being insignificant [17], however, even when respective concentrations and rate coefficients were deliberately increased. A previous comparison of experiment and model in [16] notes reasonable agreement for the C_4-species in the cyclopentene flame, which is, however, not discussed in detail.

4.3. Aromatic compounds: benzene and phenyl

With 255 nm as the ionization wavelength, different families of mass signals from species with 6–16 carbon atoms have been identified by REMPI-MBMS; Fig. 7 represents a typical REMPI mass spectrum of the cyclopentene flame at a height above burner of 2.7 mm. Possible compounds that may be the origin of these mass signals are summarized in Table 2.

That a large number of different aromatic species can be detected simultaneously at 255 nm in the REMPI experiment is explained by the temperature of the molecular beam. As shown previously in typical set-ups for mass spectrometric analysis of low-pressure flames [54], the temperature of the molecular beam is around 400 K, regardless of the starting temperature, when sampling from the flame by the quartz probe. At a temperature of 400 K, aromatic compounds exhibit broad overlapping absorption bands in the wavelength region of 210 to 270 nm, and ionization energies equal to or below 9.24 eV (see Table 2); they can thus be ionized simultaneously in this wavelength region, using a (1+1) REMPI scheme. Isomers are, however, not distinguished with this procedure. To gain additional insight into the different chemistries of the propene and cyclopentene flames and to complement the information discussed above on small stable and radical intermediates obtained by EI-MBMS, relative signal intensities for aromatic compounds were measured under identical conditions in both flames by

REMPI-MBMS. For further analysis, these REMPI signal ratios at a given mass are interpreted as mole fraction ratios in a first approximation. This was done for all mass signals shown in Table 3. As an example, Fig. 8 shows the REMPI intensity profiles for toluene (m/z = 92) and naphthalene (m/z = 128). The ratio of the observed intensity maxima, $I_{cyclopentene}/I_{propene}$, for toluene is 3.2, and the ratio for naphthalene is 6.9. Table 3 lists these experimental ratios $I_{cyclopentene}/I_{propene}$ for a number of observed aromatics, together with the corresponding ratios from the simulations with both models. For the experiment, different isomers belonging to a certain mass are not separated; in the simulations, the contributions of respective isomers were thus added to enable a comparison.

As an inset in Fig. 8, the laser intensity for the measurements in both flames is shown, indicating a variation of not more than 5%. The mass spectra were thus analyzed without any further correction to laser intensity. For further discussion of the problem of calibrating REMPI mass spectra to laser intensities, we refer to [56]. There, the entire $^1B_2 \leftarrow {}^1A_1\ 0^0_0$ transition for toluene was measured with a (1+1) REMPI process for four different laser intensities. For each wavelength in the measured spectra, a double-logarithmic plot of signal intensity of the toluene mass signal versus laser intensity was taken to evaluate the order of the ionization process. Interestingly, the order of a (1+1) REMPI ionization process was constant over the entire $^1B_2 \leftarrow {}^1A_1\ 0^0_0$ transition of toluene with a value of ~2. As a consequence, R2PI spectra can be calibrated for an entire transition band by just one factor. We therefore consider the analysis of intensity ratios as justified for the further discussion.

The formation of benzene and phenyl as representatives of a six-membered ring is considered as a key step on the way from small fuel hydrocarbons to higher PAHs and to soot. The comparison between measured and predicted concentration profiles of benzene and phenyl is displayed in Figs. 9 and 10, respectively, for both flames. Because of the central role of benzene and of the importance of unambiguously linking the results for small benzene precursors, measured by EI-MBMS, and for aromatic species, measured by REMPI-MBMS, the benzene concentration was quantitatively measured with both techniques in both flames. The agreement between the two sets of independent measurements shown in Fig. 9 is excellent in the propene flame, and also very good in the cyclopentene flame.

Benzene concentrations are calculated by both models to be about two orders of magnitude higher than those of phenyl radicals, for both investigated flames. Experimentally, a ratio of about 20 is found for the cyclopentene flame, whereas for the propene flame, measured phenyl concentrations are only about a factor of 4 lower that those of benzene. All observed species profiles exhibit a peak that is reasonably well reproduced by the predictions. For the cyclopentene flame, measured benzene profiles (Fig. 9) are matched excellently by both models, regarding shape and absolute values, whereas in the

propene flame, the agreement for benzene is not as good. Calculated maximum mole fractions agree for the MIT mechanism and are higher by a factor of 4 with the DLR mechanism, while the maximum is predicted at somewhat higher HAB in both cases. Note that no shifts were used in the modeling to account for cooling of the flame by the sampling nozzle.

The influence of the propargyl recombination reaction on the prediction of the benzene concentration in both flames will be discussed in more detail in Section 4.5.3, especially considering different rate expressions for this important reaction. Concerning phenyl radicals (Fig. 10), the experimental profile is underpredicted and simulated profiles show peak locations slightly different from the measured ones. A more detailed analysis of these results is provided in Section 4.5.4.

Overall, the agreement between experiment and model is better for benzene when the MIT model is used and for phenyl when the DLR model is used. Regarding the concentration ratio for benzene in Table 3, the MIT model is with 3.4, in very good agreement with the experimental value of 3.5±0.4, whereas the DLR model is with 0.82 much lower. It is interesting that the discrepancy between experiment and calculations in the *ratio* of the benzene mole fraction— which one would expect to be similarly affected in each of the two flames by the same key benzene-forming and -consuming reaction sequences—may be as large as a factor of 4, depending on the model used. Since the experimental error in the mole fraction ratio for benzene is only about 20–30% (see the good agreement of measured absolute benzene profiles with two different ionization techniques represented for both flames in Fig. 9), different contributing reaction pathways—potentially different for both mechanisms—must be at the origin of this discrepancy. Note also that benzene was identified by its REMPI spectrum and calibrated with a sample of known concentration, so that contributions from different C6H6 isomers (especially fulvene) do not need to be considered in this case.

4.4. Aromatic compounds: larger PAHs

Considering the differences in intensity and concentration ratios between experiment and the two reaction mechanisms observed already for the first stable aromatic species, benzene, it is of interest to pursue this behavior for the formation of larger PAHs. In Fig. 11, concentration profiles are given for the two-ring aromatic naphthalene (A2, $C_{10}H_8$) and for two one-aromatic-ring compounds with a hydrocarbon side chain, phenylacetylene ($A1C_2H$, C_8H_6) and styrene ($A1C_2H_3$, C_8H_8), whose further growth can lead to naphthalene. Experimental values are from [17,27] for the propene and from [25] for the cyclopentene flame; given the difficulties in absolute calibration for these species, the experimental error in the absolute values is estimated to be about a factor of 2–3, with the mole fraction ratio being substantially more accurate. The predictions differ for the two investigated flames

(note the logarithmic scale); also, experimental data for styrene are not available. For the propene flame, the experimental data are higher than the calculated ones. The species profiles predicted by the DLR reaction model show a pronounced maximum behavior, in accordance with the measurements; their peak values agree within about a factor of 5. Furthermore, the positions of the maxima for phenylacetylene and naphthalene and their relative concentrations agree with the experimental findings. In contrast, the species profiles obtained by the MIT reaction model are significantly lower than the experimental data—in particular for naphthalene—and the maxima are less pronounced. For the cyclopentene flame, the predicted shapes obtained with the two reaction models are similar, with the exception of styrene, which is shifted toward lesser height when the DLR mechanism is used. Although reasonable agreement is reached regarding the position and shape of the profiles, a quantitative comparison reveals distinct differences. Naphthalene is overestimated by approximately two orders of magnitude, which is even more pronounced using the MIT model. Phenylacetylene is matched reasonably well by the DLR model concerning shape, position, and peak value. Overall, these three larger species beyond benzene seem to be better represented by the latter mechanism.

Trends in the formation of larger PAHs can be discussed regarding Table 3, which presents ratios $I_{\text{cyclopentene}}/I_{\text{propene}}$ for the entire mass range studied here, together with the results from the simulations (sums for different isomers are indicated). It is interesting already at first inspection that all species studied in the experiment are more abundant in the cyclopentene flame, and that there is no simple relationship—constant ratio or linear increase—with molecular size. For a better overview, $I_{\text{cyclopentene}}/I_{\text{propene}}$ is shown in Fig. 12 as a function of mass, together with the calculated ratios from both models; note the logarithmic scale. In the experiment, the ratio varies between about 2 and 7 over the entire mass range from m/z = 78 to m/z = 202 (see also Table 3). In the lower mass range, the DLR mechanism underestimates this ratio, while the MIT predictions show a tendency to overprediction and are slightly closer to the experimental results. For species beyond benzene, including toluene (m/z = 92), phenylacetylene (m/z = 102), indene (m/z = 116), and naphthalene (m/z = 128), as well as higher mass aromatics, the MIT model disagrees increasingly, by up to three orders of magnitude, and the predictions with the DLR mechanism are also much, but not as excessively, too high. In view of these huge discrepancies, some of these ratios have been measured independently at the mass spectrometer setup at the Advanced Light Source in Berkeley, using ionization with tunable single-photon vacuum ultraviolet (synchrotron) radiation in a fully independent apparatus, and have been found in excellent agreement with the REMPI-MBMS results [57]. Note that the agreement between EI-MBMS and VUV-PI-MBMS is also in general quite satisfactory, as shown in recent measurements of absolute species concentrations in both flames [28,29].

The striking discrepancies between experiments on the one hand and modeling on the other need further analysis. Overestimation of the concentration ratio for a given mass could be caused either by underprediction of the related species in the propene flame or by overprediction of the same species in the cyclopentene flame, or both; similarly, underestimation of the ratio could be reached inversely by overprediction of the mole fraction of a given species in the propene flame or underprediction of the same species in the cyclopentene flame, or both. Although temperatures and cooling effects are different for the two fuels, this cannot be the only reason, given the large differences in predictions of the ratios by the two mechanisms. This is more surprising since both mechanisms are in quite good agreement with each other and with the experimental results for major species and small intermediates, including benzene precursors and species, which are known to be involved in PAH growth. However, it should be kept in mind that both mechanisms contain a large number of species and reactions, which are not necessarily identical. Missing pathways and incomplete knowledge of thermodynamic and kinetic data may pose severe limitations for a predictive analysis of the complex flame chemistry in fuel-rich combustion. Recent identification of a wealth of isomeric structures in the cyclopentene flame by VUV-PI-MBMS [28] illustrates this problem, since such identified species have either not been seen in a flame before, and/or their function in the reaction network is not known. The present work may thus be understood as an attempt to demonstrate to which extent small aromatics can be reliably predicted with consistently developed and constantly validated reaction models.

In the following part, we will thus discuss the model predictions with the aid of rate of production and sensitivity analyses. These will be shown for benzene, toluene, phenylacetylene, indene, and naphthalene, as these species present some representative examples in the PAH growth process. In this context, the role of the recombination of propargyl radicals to benzene and the decomposition of cyclopentadiene and its radical will be discussed in more detail. The reaction flux and sensitivity analyses were always performed near heights where maximum intermediate concentrations were observed in the flame front (HAB = 4.5 mm for the propene and HAB = 3.5 mm for the cyclopentene flame). The respective material is presented in four-panel diagrams that are always organized in the same fashion: left panels show the simulated results for the propene, right panels those for the cyclopentene flame, top panels represent calculations with the DLR, bottom panels those with the MIT mechanism. The most influential 6–10 reactions are indicated in each case; species are abbreviated as used in the respective model.

4.5. The ratio of signal intensities for benzene

To summarize the observations for benzene briefly, we refer back to the comparison between measured and predicted concentrations in Fig. 9. For the cyclopentene flame, the measured profiles were estimated well by the model calculations, both by shape and height, whereas for the propene

flame, the benzene profile is overpredicted by the DLR model by about a factor of 4. Thus, the experimental intensity ratio of 3.5 was matched considerably better by the MIT reaction model, but underestimated by the DLR reaction model (see Table 3). Previous analysis of the rates of formation and destruction of benzene from the measured intermediate concentrations in both flames and those of several other fuels [24,25,27, 30] show C_3-species recombination reactions to be of predominant importance in the propene flame, while reactions of C_2-, C_4-, and C_5-species are less significant [24,27,30]. Also, the reaction of phenyl with hydrogen atoms was seen to contribute to benzene formation. Benzene is consumed by reactions with H and OH [27]. The pattern was noted to be different for the cyclopentene flame [25,30], where propargyl recombination was also seen to be important, but where addition of CH_3 to C_5H_6 may contribute, due to the higher C_5-species concentrations [25].

4.5.1. Reaction flux analysis

The results of the reaction flux analysis for benzene are given in Fig. 13. Benzene is produced predominantly via the recombination of two propargyl radicals (R23). This is true for both investigated flames and for both reaction models. In the DLR mechanism, further important benzene production pathways are—for both flames—the recombination of phenyl radicals and H atoms (R26) and the decomposition of styrene (R27):

$2C_3H_3 \rightarrow A1,$ (R23)

$A1- + H \rightarrow A1,$ (R26)

$A1C_2H_3 \rightarrow A1 + C_2H_2.$ (R27)

In the MIT model, the recombination of propargyl according to reaction (R23) is the only benzene formation pathway in the propene flame, whereas for the cyclopentene flame, conversion of fulvene (C_6H_6f) leads to further benzene production; this pathway is not included in the DLR mechanism.

While the production channels are somewhat similar, the most important benzene consumption pathways differ for both investigated flames. Concerning the propene flame, benzene is consumed by C_2H_2 in the DLR model (R–27), leading to styrene and thus initiating the growth of larger PAHs. Furthermore, benzene decays in bothmechanisms by abstraction reactions with H and OH radicals (R31, R32), leading to phenyl. Reaction (R–27) does not play as important a role in benzene destruction in the cyclopentene flame, regardless of which of the two reaction schemes is used; here, the decay into two propargyl radicals (R–23) is identified as the dominant destruction route:

$A1 + C_2H_2 \rightarrow A1C_2H_3,$ (R–27)

$A1 + H \rightarrow A1- + H_2,$ (R31)

$A1 + OH \rightarrow A1- + H_2O$, (R32)

$A1 \rightarrow 2C_3H_3$. (R–23)

With regard to the benzene ratio, the situation seems similar in both models for the cyclopentene flame, with benzene consumption leading back into the pool of smaller radicals, whereas in the propene flame, benzene is consumed to form higher aromatics more easily in the DLR model.

4.5.2. Sensitivity analysis

The sensitivity analysis in Fig. 14 shows the importance of reactions with species derived directly from the respective fuel, such as C_3H_6, C_3H_5, C_3H_4, and C_3H_3 in the propene flame and cC_5H_6 and cC_5H_5 for the cyclopentene flame. In addition, C_3Hx -reactions are also noted in the latter flame, because the decomposition of cC_5H_5 radicals leads to the formation of propargyl and acetylene, according to the measurements of Roy et al. [39]. Since more benzene is observed when more propargyl radicals are produced, it is not surprising that the ratio between the two possible decomposition channels of propene (R12, R13) is also sensitive, the latter being an additional decay channel that diminishes the production of propargyl. Also important are further reactions of C_3H_4 species (R17–R21):

$C_3H_6 \rightarrow C_3H_5 + H$, (R12)

$C_3H_6 \rightarrow C_2H_3 + CH_3$, (R13)

$pC_3H_4 \rightarrow C_3H_3 + H$, (R17)

$C_3H_3 + H \rightarrow pC_3H_4$, (R–17)

$aC_3H_4 \rightarrow C_3H_3 + H$, (R18)

$C_3H_3 + H \rightarrow C_3H_2 + H_2$, (R25)

$pC_3H_4 + H \rightarrow C_2H_2 + CH_3$, (R19)

$pC_3H_4 + H \rightarrow C_3H_3 + H_2$, (R20)

$pC_3H_4 + OH \rightarrow C_3H_3 + H_2O$. (R21)

It is obvious that, among others, propargyl reactions are of significant importance for both flames and in both mechanisms. Potential differences between DLR and MIT model merit further analysis.

4.5.3. The influence of the recombination of propargyl radicals

Experimental propargyl profiles are quite well predicted by the DLR model: their shape is reasonably well matched. They are underestimated by less than a factor of 2 for the propene flame, and overestimated by a factor of 4 for the cyclopentene flame (see Fig. 4). Since propargyl radicals play

such an important role in the benzene profile, simulations were performed with different values for the rate coefficient of the propargyl recombination reaction from the recent literature (see Table 4); results of these calculations are given in Fig. 15.

As a basis for this work ("original DLR model"), we have used the rate coefficient for the recombination reaction of the propargyl radical (R23) determined by Scherer et al. [43] from direct shock tube measurements at high temperatures around 1.7 bar, where time-resolved resonance absorption of hydrogen atoms was sensitively observed. The initial concentration of propargyl was determined in situ by measuring the detected resonance absorption signal of iodine atoms. Since the present study is conducted in the low-pressure regime, we have chosen an intermediate value of 6.0×10^{12} cm^3 mol^{-}1 s^{-1} from [43] (where the rate coefficient is given as 4.5×10^{12} cm^3 mol^{-1} s^{-1} < k (R23) < 9×10^{12} cm^3 mol^{-1} s^{-1}), in accordance with the result for a negligible pressure dependence reported in [58].

The benzene profile was predicted to be about 50% lower in the propene flame when the value from [58] was used in the DLR model, in slightly better agreement with experiment. For the cyclopentene flame, the respective change is not as important, with about a 25% difference. Since the change is in the same direction, the resulting ratio for benzene (Table 3) would increase only slightly, from 0.82 to 1.0. Similarly, the benzene profile calculated with the DLR model was about 30% lower when the rate coefficient for (R23) from the MIT model was used (not shown in Fig. 15). If, on the other hand, the rate coefficient for (R23) used in the DLR model was implemented into the MIT model, the resulting benzene profile was about 30% higher in both flames (see Fig. 15), still in quite good agreement with experiment in both ratio and absolute concentrations. As a conclusion of this variation, it seems unlikely that remaining uncertainties in the rate expression for the propargyl recombination reaction alone are at the origin of the tendency of the DLR model to underpredict the benzene mole fraction ratio in the cyclopentene versus the propene flame. This may be understood from the importance of this reaction for the benzene concentration profiles in both flames, as seen in the reaction flux and sensitivity analyses (Figs. 13, 14). The variation of the rate coefficient affects the benzene profiles in both flames in the same direction, which causes a lesser effect on the concentration ratio.

With respect to the formation of higher-mass PAHs, it seems also unexpected and highly unlikely that the change of a single rate coefficient would lead to a better agreement in the entire mass range. Thus, further details of the PAH precursor chemistry are inspected in more detail.

From the flux analysis for propargyl (Fig. 16) and the corresponding sensitivity analysis (Fig. 17) carried out for both flames with both reaction models, only reactions that are directly connected to the propargyl radical are identified as the main important ones. However, only a minor fraction of propargyl leads to benzene formation (Fig. 16), whereas the H-abstraction reaction (R25) is a dominant propargyl consumption reaction for both mechanisms. The propargyl recombination rate (R23) reveals a stronger sensitivity for the calculations using the MIT model, probably because of the lower value of the rate coefficient. Furthermore, propargyl production from C5H5 dissociation appears to be rather slow, in particular for the cyclopentene flame.

4.5.4. The role of phenyl radicals

In both flames, phenyl radicals play an important role with respect to the rate and height of the calculated benzene profile. Several major production and consumption pathways of benzene involve phenyl radicals. The measured phenyl profiles are best predicted by the DLR model for the cyclopentene flame, although they are underestimated for both investigated flames with both models (see Fig. 10).

Phenyl (A1–, C_6H_5) is mainly formed by bimolecular H-abstraction reactions of benzene (R31, R32), and to a minor extent by the thermal decomposition of benzene; also, further radical abstraction reactions, in particular of phenylacetylene (R34, R35), and the reaction of two propargyl radicals (R24) are involved in phenyl formation:

$A1 + H \rightarrow A1- + H_2$, (R31)

$A1 + OH \rightarrow A1- + H_2O$, (R32)

$C_7H_7 + H \rightarrow A1- + CH_3$, (R–33)

$2C_3H_3 \rightarrow A1- + H$, (R24)

$A1C_2H + H \rightarrow A1- + C_2H_2$, (R34)

$A1C_2H + C_2H \rightarrow A1- + C_4H_2$. (R35)

Phenyl is mainly consumed by the following reactions, with (R26, R33) for the propene flame and with (R33) for the cyclopentene flame as the dominant destruction pathway:

$A1- + H \rightarrow A1$, (R26)

$A1- + CH_3 \rightarrow C_7H_7 + H$, (R33)

$A1- + CH_3 \rightarrow C_7H_8$, (R38)

$A1- + O_2 \rightarrow C_6H_5O + O$, (R37)

$A1- + H \rightarrow 2C_3H_3$, (R–24)

$A1- \longrightarrow C_4H_3u + C_2H_2$. (R36)

The phenyl radical thus takes part in both benzene and propargyl reaction sequences. It should be noted here that the MIT mechanism exhibits some differences with regard to the DLR mechanism highlighted above. For example, (R24) is about a factor of 20 less important than benzene formation from propargyl recombination in the DLR mechanism, while this reaction is not included in the MIT mechanism. The phenyl decomposition and isomerization reaction expressions in the DLR model are taken from shock tube experiments, while those in the MIT model are from quantum chemical calculations. The reaction flux analysis for phenyl also reveals different reaction sequences for both models; for example, the reactions of C_6H_5CHO to C_6H_5CO and further to C_6H_5 +CO in the MIT mechanism have no counterpart in the DLR mechanism, where benzaldehyde is not included as a species.

4.6. The ratio of signal intensities for toluene

For toluene (C_7H_8, *m/z* = 92), the experimental ratio is 3.2, and the DLR model predicts a value of 0.89; both ratios are similar to those for benzene. In contrast, the MIT model predicts a 4 times higher mole fraction ratio for toluene than for benzene (see Table 3).

For the propene flame, the toluene profile predicted with the DLR model is about a factor of 10 higher than that predicted by the MIT model, but with the maximum at the same position. However, for the cyclopentene flame, the toluene profile resulting from the DLR model is about 30% lower than that calculated by using the MIT model; in addition, its maximum value is reached at a higher HAB.

4.6.1. Reaction flux analysis

The main production and destruction pathways of toluene are the same for both types of flame (see Fig. 18), regardless which reaction model was used. Toluene is formed dominantly via the recombination reaction of benzyl with H atoms (R39) and by the reaction with methyl radicals, either with phenyl as in the DLR model (R38) or with benzene (MIT model, R40):

$C_7H_7 + H \rightarrow C_7H_8$, (R39)

$A1- + CH_3 \rightarrow C_7H_8$, (R38)

$A1 + CH_3 \rightarrow C_7H_8 + H$. (R40)

The decomposition of toluene according to (R–39) is the main consumption pathway for toluene, followed by reactions with H atoms (R41, R–40). The second possible decomposition pathway,

leading to phenyl and methyl radicals (R–38), may also play a role. For the thermal decay of toluene, as well as for its recombination and abstraction reactions with H radicals, the Arrhenius expressions from the experimental high-temperature shock tube work from [40] were used:

$C_7H_8 \rightarrow C_7H_7 + H$, (R–39)

$C_7H_8 + H \rightarrow C_7H_7 + H_2$, (R41)

$C_7H_8 + H \rightarrow A1 + CH_3$, (R–40)

$C_7H_8 \rightarrow A1- + CH_3$. (R–38)

4.6.2. Sensitivity analysis

For the toluene formation and destruction in the propene flame, reactions of propargyl radicals are very important, in addition to reactions involving benzyl radicals. The sensitivity analysis for the cyclopentene flame reveals the importance of reactions of cyclopentadiene and its radical cC_5H_5 (see Fig. 19). Again, the rate expressions in the DLR model for these reactions were taken from sensitive high-temperature shock tube experiments and have been used in previous modeling studies of soot formation in high-pressure systems (see information on the structure of the model in [9] and further references therein). Sensitive toluene formation reactions include the following:

$C_7H_7 + H \rightarrow C_7H_8$, (R39)

$A1- + CH_3 \rightarrow C_7H_8$, (R38)

$A1 + CH_3 \rightarrow C_7H_8 + H$. (R40)

While the influences of propargyl recombination and of cyclic C_5-species, as well as of benzyl radicals, are seen in both models, details in the sensitivity patterns are different. For example, a sensitivity to reactions involving benzyl and its decay to vinylacetylene is seen for both flames in the MIT model, whereas C_4-species are not of major influence on toluene formation and destruction in the DLR model.

4.6.3. The role of benzyl radicals

Since the decomposition of benzyl (C_7H_7) reveals a strong sensitivity to the concentration profile of toluene, its role was investigated in more detail. According to the reaction flux analysis (Fig. 20), benzyl radicals are mostly produced via three reactions, which differ somewhat for the two reaction models; the DLR model shows benzyl formation in both flames occurring predominantly through:

$A1- + CH_3 \rightarrow C_7H_7 + H$, (R33)

$C_7H_8 + H \rightarrow C_7H_7 + H_2$, (R41)

$C_7H_8 \rightarrow C_7H_7 + H.$ (R–39)

Furthermore, benzyl radicals take part in combinative reactions, including those with propargyl (R42) and acetylene (R43), which lead directly to aromatic species with a larger number of condensed rings:

$C_7H_7 + C_3H_3 \rightarrow C_{10}H_8 + 2H,$ (R42)

$C_7H_7 + C_2H_2 \rightarrow \text{indene} + H.$ (R43)

It should be noted that the decomposition products of benzyl have not yet been unambiguously identified by direct experiments. The high-temperature decomposition of benzyl has been investigated recently in a shock tube study [59], using absorption at 266 nm to detect benzyl radicals, and a valuable discussion of previous work is given in this paper. While most related studies agree in the H atom production stoichiometry, which is consistent with the decomposition to a product C_7H_6 of yet unknown structure (R44), it remains unclear whether a second channel (R45) may also contribute:

$C_7H_7 \rightarrow C_7H_6 + H,$ (R44)

$C_7H_7 \rightarrow C_4H_4 + C_3H_3.$ (R45)

Differences regarding benzyl decomposition might thus be the reason that toluene is predicted in much higher concentrations by the DLR model, and that the predicted maximum signal intensity ratio $I_{\text{cyclopentene}}/I_{\text{propene}}$ differs considerably between the two reaction models.

4.7. The ratio of signal intensities for phenylacetylene

The ratio $I_{\text{cyclopentene}}/I_{\text{propene}}$ calculated for phenylacetylene ($A1C_2H$, m/z = 102) by the DLR model is 8.1, close to the experimental value of 5.3, while that obtained with the MIT model is approximately 70 times higher (see Table 3).

Phenylacetylene is matched quite well using the DLR model concerning shape, position, and peak value for both flames (see Fig. 11). The species profiles predicted by the MIT model are considerably lower for the investigated propene flame and higher for the cyclopentene flame. Although the accuracy of the absolute mole fractions in Fig. 11, which have been measured by EI-MBMS [17], may be limited because of calibration and sensitivity issues, it is interesting to analyze these data with respect to the concentration ratio in the cyclopentene versus the propene flame; here, a value of 2.3 is obtained from this fully independent measurement, which is in reasonable agreement with the prediction with the DLR model, and deviates more than an order of magnitude from that obtained with the MIT model.

4.7.1. Reaction flux analysis

The main reactions responsible for the formation as well as the destruction of phenylacetylene differ for the two flames as well as for the used reaction model (see Fig. 21). For the DLR model, mainly reactions with acetylenic species are important for the propene flame (R–34, R–35, and R28) and reactions of the phenylacetylene radical $A1C_2H^*$ (R46, R47) in the case of the cyclopentene flame. In the MIT model, reactions with oxygenic species such as O, OH, and H_2O turned out to be of greater importance:

$A1- + C_2H_2 \rightarrow A1C_2H + H,$ (R–34)

$A1- + C_4H_2 \rightarrow A1C_2H + C_2H,$ (R–35)

$A1 + C_2H_2 \rightarrow A1C_2H + H_2,$ (R28)

$A1C_2H^* + H \rightarrow A1C_2H,$ (R46)

$A1C_2H^* + H_2 \rightarrow A1C_2H + H.$ (R47)

4.7.2. Sensitivity analysis

The sensitivity analysis for the formation and destruction of phenylacetylene shown in Fig. 22, reveals that for the propene flame, reactions involving propargyl radicals (as aromatics precursors) as well as phenyl and benzene (as products from phenylacetylene reactions) are dominant. This is observed for both reaction models. For the cyclopentene flame, both reaction models show the great importance of reactions including cyclic C_5-species. It should be noted that the combination reaction between two cyclopentadienyl radicals leading to naphthalene (R50) is the most sensitive reaction in this flame, which emphasizes the importance of the cyclic C_5H_6/C_5H_5 chemistry. However, this reaction has not yet been studied experimentally for the relevant conditions:

$2cC_5H_5 \rightarrow C_{10}H_8 + 2H.$ (R50)

In summary, using the experimentally derived rate expressions for the decomposition of phenylacetylene, cyclopentadiene and cyclopentadienyl radicals as well as the oxidation reactions of these compounds in conjunction with the propargyl reactions (its recombination, its decomposition, and the H-abstraction reaction) used in the DLR model seems to lead to a much better prediction of the experimentally determined concentration profile of phenylacetylene.

4.8. The ratio of signal intensities for styrene

For styrene ($A1C_2H_3$, m/z = 104), the experimentally derived ratio $I_{cyclopentene}/I_{propene}$ is relatively close to the values predicted by both reaction models. However, the calculated concentration profiles differ considerably for both investigated flames: using the DLR reaction model, much higher concentrations

are predicted and—additionally—at a lesser height above the burner (see Fig. 11). But since the trend is the same for both types of flames, the ratio $I_{cyclopentene}/I_{propene}$ remains the same.

4.8.1. Reaction flux analysis

Only a very few reactions dominate the height of the concentration profile (see Fig. 23). According to the DLR mechanism, styrene is produced almost exclusively via the recombination reaction (R–27), whereas in the MIT model, bimolecular reactions of the HACA type are identified as the most important ones. The decomposition of styrene (R27) is by far the most effective destruction route for styrene for both flames and both reaction models:

$A1 + C_2H_2 \rightarrow A1C_2H_3,$ (R–27)

$A1– + C_2H_4 \rightarrow A1C_2H_3 + H,$ (R30)

$A1 + C_2H_3 \rightarrow A1C_2H_3 + H,$ (R29)

$A1C_2H_3 \rightarrow A1 + C_2H_2.$ (R27)

4.8.2. Sensitivity analysis

The reactions (R27) and (R–27) are very sensitive regarding the formation and production of styrene, besides reactions that produce propargyl radicals and benzene (see Fig. 24). This is clearly demonstrated in case of the propene flame. For the cyclopentene flame, reactions of the cC_5H_6/cC_5H_5-system are also important. This reflects the competition between the formation of propargyl radicals and hence benzene or phenyl, or the alternative direct pathway leading to higher condensed species, via a combinative reaction such as

$2cC_5H_5 \rightarrow C_{10}H_8 + 2H.$ (R50)

4.9. The ratio of signal intensities for indene

For indene (C_9H_8, m/z = 116), the experimental value for the ratio $I_{cyclopentene}/I_{propene}$ is much lower than those obtained by the simulations. The DLR model provides an approximately 30 times higher ratio, and an even higher value—about 450 times higher than measured—results when the MIT model is used (see Table 3). The difference between the two models can be understood in terms of the calculated concentration profiles (not shown). For the propene flame, the MIT model predicts a concentration profile of indene that is about 30 times lower than that obtained using the DLR model, whereas for the cyclopentene flame, the model calculations differ only by a factor of 2.5. Again, the DLR model predicts a higher concentration, with the maximum value at a slightly higher height above the burner surface.

4.9.1. Reaction flux analysis

Indene is formed almost exclusively via recombination of H atoms with indenyl (R48), for both flames, regardless which of the two reaction models was used. More specifically, the concentration profile of indene calculated with the DLR mechanism for the propene flame reveals relatively high values, which suggests consideration of the respective consumption reactions. Here, the H-abstraction reaction of indene (R49) is a major consumption pathway, besides the decomposition reaction to H and indenyl (R–48):

indenyl + H→indene, (R48)

Indene + H→indenyl + H_2, (R49)

Indene→indenyl + H. (R–48)

4.9.2. Sensitivity analysis

Several reactions exhibit relatively high sensitivity with respect to the formation of indene, as shown in Fig. 25. In the propene flame, reactions involving propargyl and other C_3-species are dominant in the DLR mechanism, and benzyl radicals are also involved, especially regarding the MIT model. Respective production and destruction routes include reactions (R33), (R–45), and (R43). There is a competition between benzyl and further smaller hydrocarbon species leading either to indene or to naphthalene (R42), and it is noted that the DLR model provides higher benzyl concentrations than the MIT model (not shown):

A1– + CH_3 →C_7H_7 + H, (R33)

C_4H_4 + C_3H_3 →C_7H_7, (R–45)

C_7H_7 + C_3H_3 →$C_{10}H_8$ + 2H, (R42)

C_7H_7 + C_2H_2 →indene + H. (R43)

For the cyclopentene flame, reactions of *c*C_5H_6- and *c*C_5H_5-species are found to be sensitive. Hence, their further kinetics is important with respect to the formation of larger PAHs. It is of particular interest whether *c*C_5H_5 isomerizes to open-chained C_5H_5 species that will decompose fast to propargyl and acetylene (sequence a) or whether they will react directly to naphthalene (sequence b):

cC_5H_6 →*c*C_5H_5 →*I* -C_5H_5 →C_3H_3 + C_2H_2

(sequence a),

2*c*C_5H_6 →2*c*C_5H_5 →$C_{10}H_8$ + 2H

(sequence b).

The cyclopentene flame produces very rapidly a large amount of *c*C_5H_6- and *c*C_5H_5-species (see Fig. 26), in accordance with the calculations. The agreement between measured and predicted species profiles using the DLR reaction model in this flame is excellent, with respect to both the height and shape of the experimental data, while it is less satisfactory with both models in the propene flame where these C_5-species are not major intermediates. The MIT model overestimates the *c*C_5H_5 concentration in the cyclopentene flame by almost an order of magnitude, also predicting a much broader profile than measured, and the *c*C_5H_6 profile by a factor of 4. The rate expressions for these particular reactions in the DLR mechanism were taken from a direct investigation at high temperatures [39]. It should be mentioned that also for the propene flame, the experimental profiles are better matched by the DLR model, in particular for *c*C_5H_6 (Fig. 26). Key reactions include

cC_5H_6 →*c*C_5H_5 + H, (R57)

cC_5H_6 + H→*c*C_5H_5 + H_2, (R58)

cC_5H_5 →*I* -C_5H_5, (R59)

I -C_5H_5 →C_3H_3 + C_2H_2, (R60)

2*c*C_5H_5 →$C_{10}H_8$ + 2H. (R50)

The observation of a better agreement of the DLR model prediction for indene with the measured intensity ratio $I_{cyclopentene}/I_{propene}$ may be a result of consequently using experimentally obtained rate expressions for the reactions of relevant species including propargyl, benzyl, toluene, cyclopentadiene and cyclopentadienyl, as well as phenylacetylene, that were identified as intermediates in the main reaction routes. In particular, accurate rate expressions for reactions in the C_5-system are seen to be important for the prediction of indene concentrations and their ratio in the two flames.

4.10. The ratio of signal intensities for naphthalene

To predict soot formation with a kinetic model, it is crucial to correctly describe the formation of further condensed ring systems such as naphthalene ($C_{10}H_8$, *m/z* = 128). The ratio of the signal intensity measured at the maxima in the two investigated flames is with a value of 6.9, much lower than those obtained by the modeling calculations (see Table 3), and it is close to the ratio $I_{cyclopentene}/I_{propene}$ of 6.5 measured for indene. The DLR model leads to an approximately 45 times higher value, which is only slightly higher than that obtained for indene. Concerning the MIT model, a value is reached that is more than 3 orders of magnitude higher than the experimental one, and about a factor of 6 higher than that for indene using the same model. An estimate from the measured concentrations for naphthalene by EI-MBMS displayed in Fig. 11 provides a ratio on the order of 1–2, which is less accurate than the ratio determined by REMPI-MBMS because of the sensitivity and calibration problems mentioned before, but is of the same order of magnitude. Similarly, an

independent measurement using vacuum UV photoionization provided a ratio of 8.5 [57], in good agreement with that measured by REMPI-MBMS.

The observed pronounced disagreements with the experimental findings raise some concern, since naphthalene as a two-ring aromatic species finds itself at the initial stages of molecular growth, and an accurate prediction would be a prerequisite for a reliable transition from the molecular gas-phase kinetic mechanism to the soot submodel.

The observations might be explained by the predicted naphthalene profiles (see Fig. 11), which differ for the two investigated flames. Concerning the cyclopentene flame, the calculated profiles are more than two orders of magnitude higher than the experimental ones when the MIT model is used, although the position and shape of the measured naphthalene profile are quite well matched. In contrast, for the propene flame, the calculated values are lower than the experimental ones by almost an order of magnitude, thus leading to an overprediction of the ratio by a factor of about 2500. The DLR reaction model matches the experimental profiles within about a factor of 5 for the propene flame and 50 for the cyclopentene flame, underpredicting the naphthalene concentration in the former and overpredicting it in the latter. Both models thus show a tendency to underestimate the production of naphthalene in the propene flame and to overestimate its production and/or underestimate its consumption in the cyclopentene flame, with this tendency being more pronounced in the MIT model.

4.10.1. Reaction flux analysis

The reaction flux analysis for naphthalene is given in Fig. 27. For the propene flame, it is found that the combinative reaction of benzyl with propargyl (R42) plays an overwhelming role. This may not be surprising, since this reaction leads directly to naphthalene, compared to the HACA-type reactions, which proceed via several reaction steps—starting from benzene/phenyl—to form the two condensed rings. However, it should be emphasized that no direct measurement at high temperatures exists to date for this important reaction, and respective experiments would be a valuable addition. It seems necessary in this respect to describe the temporal behavior of benzyl radicals correctly. Furthermore, it might be useful to look for additional reactions that might be important concerning the build-up of naphthalene.

The main naphthalene consumption routes are H-abstraction reactions (R51, R52) in both reaction models and for both investigated systems:

$C_7H_7 + C_3H_3 \rightarrow C_{10}H_8 + 2H,$ (R42)

$C_{10}H_8 + H \rightarrow C_{10}H_7 + H_2$, (R51)

$C_{10}H_8 + OH \rightarrow C_{10}H_7 + H_2O$, (R52)

$C_{10}H_8 \rightarrow C_{10}H_7 + H$. (R53)

The picture differs if one refers to the cyclopentene flame, where (R42) is found to be insignificant. Besides this, however, the same reaction pathways as for the propene flame are identified as the most effective ones. It is interesting to note that the main reaction for the production of naphthalene differs for both reaction models: in the MIT model, the combinative reaction involving two $c$$C_5H_5$-radicals leading directly to naphthalene (R50) contributes much more, whereas for the DLR model, naphthalene is mainly formed via the recombination of H with naphthyl radicals (R–53) and by H-abstraction reaction with napththol (R56):

$C_{10}H_7 + H \rightarrow C_{10}H_8$, (R–53)

$2c C_5H_5 \rightarrow C_{10}H_8 + 2H$, (R50)

$C_{10}H_7OH + H \rightarrow C_{10}H_8 + OH$. (R56)

The naphthyl radical originates from the reaction of naphthalene with hydrogen atoms, and it is consumed with O_2 to form naphthol radicals, $C_{10}H_7O$. These may react either to naphthol, $C_{10}H_7OH$, or to indenyl and CO. Naphthol may also be formed by reaction of naphthalene with OH. These reactions are of different importance in the two flames, as seen in Fig. 27.

4.10.2. Sensitivity analysis

The sensitivity analysis for naphthalene in Fig. 28 shows the importance of the break-up of the investigated fuel. In both models, the calculations identified reactions involving propargyl and further C_3H_x - species as well as benzyl formation reactions for the propene flame. Similarly, reactions of $c$$C_5H_x$ -species were seen to be the most sensitive ones for naphthalene formation and consumption in the cyclopentene flame:

A1– + $CH_3 \rightarrow C_7H_7 + H$, (R33)

$C_7H_7 + C_3H_3 \rightarrow C_{10}H_8 + 2H$, (R42)

$2c C_5H_5 \rightarrow C_{10}H_8 + 2H$, (R50)

$c C_5H_6 \rightarrow c C_5H_5 + H$, (R57)

$c C_5H_6 + H \rightarrow c C_5H_5 + H_2$. (R58)

However, these reactions (R57, R58) are considered to be well studied—with the exceptions of (R42) and (R50)—since direct high-temperature shock tube experiments exist, although carried out at elevated pressure of about 2 bar [39]. Thus, to improve the agreement between experimental and

calculated values for the ratio $I_{cyclopentene}/I_{propene}$, it is suggested to analyze critically the reaction kinetics concerning the propene system. Furthermore, the oxidation reactions of propargyl as well as of c-C_5H_6 and its radical need to be determined by direct measurements at high temperatures and in the appropriate pressure regime.

In addition, it must be emphasized that only limited knowledge exists concerning the thermal decay of naphthalene and naphthyl, as well as their oxidation reactions. Moreover, the decomposition of naphthalene and naphthyl may proceed over several reaction pathways, as a result of the competition between C–C and C–H bond fission:

$$C_{10}H_8 \rightarrow C_{10}H_7 + H, \quad \text{(R53)}$$

$$C_{10}H_8 + H \rightarrow C_{10}H_7 + H_2, \quad \text{(R51)}$$

$$C_{10}H_7 \rightarrow C_{10}H_6 + H, \quad \text{(R54)}$$

$$C_{10}H_7 \rightarrow C_8H_5 + C_2H_2. \quad \text{(R55)}$$

Most of the reaction rate coefficients included in the reaction models are taken from quantum RRKM calculations (see, e.g., references in [37,50] for individual reactions). Very recently, Vöhringer and coworkers [60,61] studied the thermal decay of both naphthalene and naphthyl in the temperature range between 1350 and 2000 K at elevated pressures of 2–5 bar. The experiments were performed behind reflected shock waves. Besides time-resolved measurements of H- and I-atoms by the highly sensitive ARAS method, non-resonant absorption profiles of molecular products were recorded. In addition, residual GC-MS gas analysis of the postshock educts was performed, demonstrating the formation of acetylenic species, namely acetylene, diacetylene (C_4H_2), and— with lower concentrations—tri- and tetraacetylene. Arrhenius expressions were determined for the initial formation of H-atoms obtained during the decay of naphthalene and for the depletion of naphthalene measured by UV spectroscopy. From these measurements it was deduced that H-elimination is the dominant initiation step of the unimolecular naphthalene decomposition. However, the rate coefficients for naphthalene decomposition were about one order of magnitude higher than those from [37]. For the unimolecular decomposition of naphthyl, the values of the rate coefficient were determined to be about a factor of 15 smaller than the data from [62]. It also remains unclear whether several decay pathways are open, and if so, whether rate expressions as a function of pressure for these different product channels would have to be determined. In a recent study, experiments and quantum chemical calculations have been devoted to the 1-naphthylacetylene isomerization reaction [63], and yet unpublished results are quoted on high-temperature decomposition of naphthalene with the single-pulse shock tube technique, which permits an analysis of the main products; thus, identification of potential product channels may be on the way.

4.10.3. Comparison with modeling results in the literature

It has been noted before [16] that naphthalene concentrations in the cyclopentene flame were predicted in large excess (i.e., a factor of 35) with respect to the experimental results. This observation agrees quite well with that made here using both models (see Fig. 11), where naphthalene mole fractions were overpredicted by about a factor of 50 by the DLR model, and by about a factor of 200 by the MIT model. In the study by Lindstedt and Rizos [16], this overestimation was in part ascribed to the possibly too high rate coefficient for the cyclopentadienyl recombination reaction (R50), which has also been used here. This observation may be discussed with respect to the reaction flux and sensitivity analyses with both models, since reaction (R50) is far more important for naphthalene formation in the MIT than in the DLR model, and this might explain why the naphthalene concentration would even be more substantially overpredicted by the former. Interestingly, the measured mole fractions of cyclopentadiene and cyclopentadienyl are matched more reasonably than naphthalene by both models (see Fig. 26), with the consumption of both species by the MIT mechanism being somewhat slower, and the level of these important C_5-species considerably higher. In the propene flame, the cyclopentadienyl recombination is not of similar importance. However, naphthalene concentrations in this flame are not in agreement with the experiment either; here, an underprediction was seen in both models, with the dominant naphthalene formation reaction being that of benzyl with propargyl (R42). New information on the toluene decomposition and on the branching ratio toward benzyl or phenyl radicals from recent experiments and calculations [64,65] might be useful in an improved assessment of the importance of reaction pathways involving these two species.

Naphthalene has also been predicted in premixed, near-sooting low-pressure flames of several other fuels using the MIT mechanism, and in particular, benzene/ oxygen/argon flames have been studied experimentally and numerically by Howard, Richter, and their collaborators [52,66]. Interestingly, naphthalene concentrations are quite well predicted in the benzene flame using essentially the same reaction mechanism and kinetic data [66], using HACA type sequences and the cyclopentadienyl recombination reaction, with the latter being the predominant naphthalene source. Similar sequences are also discussed for phenanthrene formation, and the important contribution of cyclopentadienyl and phenyl radical reactions is pointed out in this investigation. Böhm et al. [17] have predicted phenylacetylene, indene, naphthalene, and phenanthrene concentrations in the propene flame investigated here, using a modeling approach that was more fully described in [67]. Good agreement of experiment and model is observed for most major and small radical species. Benzene is predominantly formed by the propargyl recombination reaction, and four different pathways are tested for naphthalene and, in particular, phenanthrene formation. For naphthalene, concentrations are overestimated by a factor of 2, and for phenanthrene, no comparison with the experiment was possible, since concentrations were below the experimental detection sensitivity. It is concluded in this study [17] that reactions that involve side-chain aromatics with C_3H_3, such as that of C_7H_7 with C_3H_3, may

play a significant role in the build-up of two- and three-membered aromatic ring structures. Also, the cyclopentadienyl recombination reaction, as well as combinative steps of the type phenyl plus benzene, are seen to make substantial contributions.

While there seems to be general agreement about the importance of some pivotal species in small aromatics formation, which may include propargyl, cyclopentadienyl, phenyl, benzyl, and aromatics with side chains such as phenylacetylene, the influence of which has thus been studied in the present investigation, reliable kinetic reaction coefficients from direct experimental studies under the relevant conditions would be crucial for a better quantitative picture. In particular, it seems that the fuel-specific aspects of the formation of small PAHs leave ample room for refinement of current models that have successfully predicted the general trends and reaction sequences toward PAH and soot formation under a wide range of conditions.

5. Conclusions

Resonance-enhanced multiphoton ionization molecular beam mass spectrometry (REMPI-MBMS) has been used to study the formation of small PAHs in non-sooting (C/O = 0.77), laminar, premixed low-pressure flames of propene and cyclopentene under identical conditions. To complement previous studies of both flames with electron impact ionization (EI-)MBMS, which have provided major species concentrations and the mole fractions of small molecular intermediates up to benzene, ratios of the maximum concentrations of species in the mass range of m/z = 78 up to approximately m/z = 200 were determined. Benzene concentrations were measured quantitatively with both techniques and were found in excellent agreement.

The experimental profiles were modeled relying on two detailed reaction schemes, one of which, the MIT mechanism, had been taken from the literature [37,50]. The other mechanism, the DLR reaction model, had been developed over the past decade for the prediction of concentration profiles of large PAHs, in particular, since they are the major soot precursors. Comparing the two investigated flames in the present work, a different set of reactions was identified to be of main importance for the prediction of species up to naphthalene, depending on the chosen fuel. For a given flame, however, the same set of reactions was identified to dominate the species profiles. Concerning the cyclopentene flame, reactions of cyclopentadienyl and cyclopentadiene were observed to be of considerable importance, whereas for the propene flame, reactions of propargyl radicals, of propene/propyne, and of acetylene were most important.

The predictions of both reaction models were studied in more detail using reaction flux and sensitivity analyses. With this, it was possible to identify the main PAH growth routes and to determine important reactions of selected species. The focus of the modeling study was on the predictions of aromatic species and of their particular precursors, including radicals such as propargyl, cyclopentadienyl, phenyl, and benzyl. For a direct comparison with the experiment, which had measured the ratio $I_{\text{cyclopentene}}/I_{\text{propene}}$ of the maximum of the signal intensity for a given mass in the cyclopentene flame versus that in the propene flame, this ratio was also calculated for every mass (if necessary as a sum of contributing isomers) by both models. Such ratios were then analyzed for a range of small aromatics involving specifically benzene, toluene, phenylacetylene, styrene, indene, and naphthalene.

It was found that above $m/z \approx 100$ this ratio is predicted by both models to be considerably higher than the measured one, in particular with increasing PAH mass. The two reaction models reveal significant differences in the values of that ratio, in particular for phenylacetylene, indene, and naphthalene. The predictions from the DLR model were found to be closer to the experimental values in this range. This was explained by a closer match of those species profiles that were identified as sensitive with respect to the formation and destruction pathways of the considered higher-mass PAHs. For these important reactions, rate expressions derived from direct measurements at high temperatures were used if possible.

Since earlier attempts to model each of the two flames individually, with particular emphasis on benzene formation pathways, substantial improvement has been noted with respect to the experimental and theoretical study of some crucial reactions, including some involving C_3-species or toluene, benzyl, and phenyl. In spite of improving knowledge, some important reactions will need further study, including in particular the combination of two cyclopentadienyl radicals (R50) or that of propargyl with benzyl (R42). With experimental techniques such as single-pulse shock tubes, shock tubes combined with mass spectrometric analysis, or high-temperature flow reactors with high temporal resolution, these and other important reactions may be accessible under well-defined conditions in the important temperature range and at different pressures. In particular, these experimental studies should not only permit an accurate determination of the kinetic behavior of the relevant species, also in the presence of oxygen, but also the reliable determination of the products and branching ratios. Finally, more direct experiments are required, concerning the determination of quantitative mole fraction profiles of larger condensed aromatic species, in particular of indene and naphthalene, under both pyrolytic and oxygen-rich conditions.

Acknowledgments

K. Kohse-Höinghaus and M. Kamphus gratefully acknowledge financial support by the Deutsche Forschungsgemeinschaft (Ko 1363/4-3, Ko 1363/18- 1, Ko 1363/18-3). The authors thank Regine Schröder for her assistance in preparing the figures and Dr. P. Frank for fruitful discussions and suggestions concerning the reaction kinetics.

References

[1] R.F. Sawyer, Proc. Combust. Inst. 24 (1992) 1423– 1432.

[2] P. Dagaut, Phys. Chem. Chem. Phys. 4 (2002) 2079– 2094.

[3] M. Frenklach, H. Wang, in: H. Bockhorn (Ed.), Soot Formation in Combustion, Springer-Verlag, Berlin, 1994, pp. 165–192.

[4] H. Richter, J.B. Howard, Prog. Energy Combust. Sci. 26 (4–6) (2000) 565–608.

[5] N.M. Marinov, W.J. Pitz, C.K. Westbrook, M.J. Castaldi, S.M. Senkan, Combust. Sci. Technol. 116– 117 (1996) 211–287.

[6] J.A. Miller, M.J. Pilling, J. Troe, Proc. Combust. Inst. 30 (2005) 43–88.

[7] D. Hu, M. Braun-Unkhoff, P. Frank, Combust. Sci. Technol. 149 (1–6) (1999) 79–94.

[8] D. Hu, M. Braun-Unkhoff, P. Frank, Z. Phys. Chem. 214 (4) (2000) 473–491.

[9] H. Böhm, M. Braun-Unkhoff, P. Frank, Prog. Comput. Fluid Dyn. 3 (2003) 145–150.

[10] H. Bockhorn (Ed.), Soot Formation in Combustion, Springer-Verlag, Berlin, 1994.

[11] C.J. Pope, J.A. Miller, Proc. Combust. Inst. 28 (2000) 1519–1527.

[12] K.H. Homann, Angew. Chem. Int. Ed. 37 (18) (1998) 2434–2451.

[13] K. Hoyermann, F. Mauß, T. Zeuch, Phys. Chem. Chem. Phys. 6 (14) (2004) 3824–3835.

[14] E. Goos, M. Braun-Unkhoff, P. Frank, Modeling of PAH formation in laminar premixed benzene-air flames, in: Proceedings of the 4th European Combustion Meeting, Louvain-la-Neuve, Belgium, 2005, No. 015.

[15] C.S. McEnally, L.D. Pfefferle, B. Atakan, K. Kohse-Höinghaus, Prog. Energy Combust. Sci. 32 (3) (2006) 247–294.

[16] R.P. Lindstedt, K.-A. Rizos, Proc. Combust. Inst. 29 (2002) 2291–2298.

[17] H. Böhm, A. Lamprecht, B. Atakan, K. Kohse-Höinghaus, Phys. Chem. Chem. Phys. 2 (21) (2000) 4956–4961.

[18] H. Wang, M. Frenklach, Combust. Flame 110 (1–2) (1997) 173–221.

[19] J. Appel, H. Bockhorn, M. Frenklach, Combust. Flame 121 (1–2) (2000) 122–136.

[20] H. Richter, W.J. Grieco, J.B. Howard, Combust. Flame 119 (1–2) (1999) 1–22.

[21] A. Ergut, S. Granata, J. Jordan, J. Carlson, J.B. Howard, H. Richter, Y.A. Levendis, Combust. Flame 144 (2006) 757–772.

[22] F. Defoeux, V. Dias, C. Renard, P.J. van Tiggelen, J. Vandooren, Proc. Combust. Inst. 30 (2005) 1407–1415.

[23] J. Ahrens, A. Keller, R. Kovacs, K.-H. Homann, Ber. Bunsenges. Phys. Chem. 102 (12) (1998) 1823–1839.

[24] A. Lamprecht, B. Atakan, K. Kohse-Höinghaus, Combust. Flame 122 (4) (2000) 483–491.

[25] A. Lamprecht, B. Atakan, K. Kohse-Höinghaus, Proc. Combust. Inst. 28 (2000) 1817–1824.

[26] A.T. Hartlieb, B. Atakan, K. Kohse-Höinghaus, Appl. Phys. B 70 (2000) 435–445.

[27] B. Atakan, A.T. Hartlieb, J. Brand, K. Kohse-Höinghaus, Proc. Combust. Inst. 27 (1998) 435–444.

[28] N. Hansen, T. Kasper, S.J. Klippenstein, P.R. Westmoreland, M.E. Law, C.A. Taatjes, K. Kohse-Höinghaus, J. Wang, T.A. Cool, J. Phys. Chem. A 111 (19) (2007) 4081–4092.

[29] K. Kohse-Höinghaus, P. Oßwald, U. Struckmeier, T. Kasper, N. Hansen, C.A. Taatjes, J. Wang, T.A. Cool, S. Gon, P.R. Westmoreland, Proc. Combust. Inst. 31 (2007) 1119–1127.

[30] B. Atakan, A. Lamprecht, K. Kohse-Höinghaus, Combust. Flame 133 (4) (2003) 431–440.

[31] L.V. Moskaleva, A.M. Mebel, M.C. Lin, Proc. Combust. Inst. 26 (1996) 521–526.

[32] C.F. Melius, M.E. Colvin, N.M. Marinov, W.J. Pitz, S.M. Senkan, Proc. Combust. Inst. 26 (1996) 685–692.

[33] R.J. Kee, F.M. Rupley, J.A. Miller, One-dimensional premixed laminar flame code, CHEMKIN-II Version 2.5b, Livermore, CA, December 1992.

[34] A. Burcat, Third Millennium Ideal Gas and Condensed Phase Thermochemical Database for Combustion, Technion Aerospace Engineering (TAE) Report #867, January 2001; or Burcat's Ideal Gas Thermochemical Database, http://garfield.elte.chem/Burcat/burcat.html.

[35] R.J. Kee, F.M. Rupley, J.A. Miller, The Chemkin Thermodynamic Database, Report SAND87-8215, Sandia National Laboratories, Livermore, CA, 1987.

[36] R.J. Kee, G. Dixon-Lewis, J. Warnatz, M.E. Coltrin, J.A. Miller, The Chemkin Transport Database, Report SAND86-8246, Sandia National Laboratories, Livermore, CA, 1986.

[37] H. Richter, J.B. Howard, http://web.mit.edu/anish/ www/MITcomb.html.

[38] Y. Tan, P. Frank, Proc. Combust. Inst. 26 (1996) 677– 684.

[39] K. Roy, C. Horn, P. Frank, V.G. Slutsky, Th. Just, Proc. Combust. Inst. 27 (1998) 329–336.

[40] M. Braun-Unkhoff, P. Frank, Th. Just, Proc. Combust. Inst. 22 (1988) 1053–1061.

[41] C. Horn, K. Roy, P. Frank, Th. Just, Proc. Combust. Inst. 27 (1998) 321–328.

[42] J. Herzler, P. Frank, Ber. Bunsenges. Phys. Chem. 96 (1992) 1333–1338.

[43] S. Scherer, Th. Just, P. Frank, Proc. Combust. Inst. 28 (2000) 1511–1518.

[44] M.B. Colket, D.J. Seery, Proc. Combust. Inst. 25 (1994) 883–891.

[45] K.P. Geigle, Y. Schneider-Kühnle, V. Krüger, M. Tsurikov, R. Lückerath, M. Braun-Unkhoff, N. Slavinskaya, P. Frank, W. Stricker, M. Aigner, Soot concentrations and temperatures for the soot model validation using laser-based diagnostics: LII and shifted vibrational CARS, in: Proceedings of the 3rd European Combustion Meeting, Orléans, France, 2003, No. 77.

[46] E. Goos, F. Douce, N. Djebaïli-Chaumeix, M. Braun- Unkhoff, N. Slavinskaya, P. Frank, C.E. Paillard, Experimental and numerical investigation focusing on early soot formation of toluene and 1-methylnaphthalene at high pressures, in: Proceedings of the 3rd European Combustion Meeting, Orléans, France, 2003, No. 210.

[47] E. Goos, M. Braun-Unkhoff, P. Frank, Modeling of PAH formation in laminar premixed flames with C1, C2 and C6 fuels, in: 30th International Symposium on Combustion, Abstracts of Work-in-Progress Posters, The Combustion Institute, Pittsburgh, 2004, p. 155.

[48] H. Richter, M. Braun-Unkhoff, S. Granata, J. Yu, E. Goos, N.A. Slavinskaya, P. Frank, W.H. Green, J.B. Howard, Computational investigation of PAH and soot formation in premixed ethylene flames, in: 4th European Combustion Meeting, Louvain-la-Neuve, Belgium, 2005, No. 163.

[49] A. El Bakali, M. Braun-Unkhoff, P. Dagaut, P. Frank, M. Cathonnet, Proc. Combust. Inst. 28 (2000) 1631– 1638.

[50] H. Richter, J.B. Howard, Phys. Chem. Chem. Phys. 4 (2002) 2038–2055.

[51] L. Dupont, A. El Bakali, J.-F. Pauwels, I. da Costa, P. Meunier, H. Richter, Combust. Flame 135 (2003) 171– 183.

[52] H. Richter, S. Granata, W.H. Green, J.B. Howard, Proc. Combust. Inst. 30 (2005) 1397–1405.

[53] J.A. Miller, C.F. Melius, Combust. Flame 91 (1) (1992) 21–39.

[54] M. Kamphus, N.-N. Liu, B. Atakan, F. Qi, A. McIlroy, Proc. Combust. Inst. 29 (2002) 2627–2633.

[55] NIST Chemistry WebBook, The National Institute of Standards and Technology (NIST), http://webbook. nist.gov/chemistry/.

[56] K. Kohse-Höinghaus, A. Schocker, T. Kasper, M. Kamphus, A. Brockhinke, Z. Phys. Chem. 219 (5) (2005) 583–599.

[57] N. Hansen, T. Kasper, P. Oßwald, T. Cool, K. Kohse-Höinghaus, unpublished results, July 2005.

[58] R.X. Fernandes, H. Hippler, M. Olzmann, Proc. Combust. Inst. 30 (2005) 1033–1038.

[59] M.A. Oehlschlaeger, D.F. Davidson, R.K. Hanson, J. Phys. Chem. A 110 (21) (2006) 6649–6653.

[60] P. Vöhringer, unpublished results, in preparation for Ph.D. thesis, Universität Stuttgart, 2007.

[61] P. Vöhringer, M. Braun-Unkhoff, P. Frank, Th. Just, Experimental investigation of the unimolecular thermal decomposition of naphthalene, in: 6th International Conference on Chemical Kinetics, Gaithersburg, MD, July 25–29, 2005, p. 150.

[62] K. Henning, Stoßwellenuntersuchungen zur Pyrolyse von Biphenylen, 1-Naphthyliodid und Methyliodid, Ph.D. thesis, Cuvillier-Verlag Göttingen, 2000.

[63] A. Lifshitz, C. Tamburu, F. Dubnikova, Proc. Combust. Inst. 31 (2007) 241–248.

[64] M.A. Oehlschlaeger, D.F. Davidson, R.K. Hanson, Proc. Combust. Inst. 31 (2007) 211–219.

[65] S.J. Klippenstein, L.B. Harding, Y. Georgievskii, Proc. Combust. Inst. 31 (2007) 221–229.

[66] H. Richter, T.G. Benish, O.A. Mazyar, W.H. Green, J.B. Howard, Proc. Combust. Inst. 28 (2000) 2609– 2618.

[67] H. Böhm, H. Jander, Phys. Chem. Chem. Phys. 1 (1999) 3775–3781.

Table 1

Additional reactions included to describe the depletion of cyclopentene; the sequence is taken from the model used in [49]

No.	Reaction	A	n	E_a
R1	$c\mathrm{C_5H_8} \leftrightarrow c\mathrm{C_5H_6} + \mathrm{H_2}$	1.58E+13	0.0	59780
R2	$c\mathrm{C_5H_8} + \mathrm{OH} \leftrightarrow c\mathrm{C_5H_7} + \mathrm{H_2O}$	4.80E+13	0.0	300
R3	$c\mathrm{C_5H_8} + \mathrm{O} \leftrightarrow c\mathrm{C_5H_7} + \mathrm{OH}$	2.78E+11	0.0	2508
R4	$c\mathrm{C_5H_8} + \mathrm{H} \leftrightarrow c\mathrm{C_5H_7} + \mathrm{H_2}$	2.80E+10	0.0	18790
R5	$c\mathrm{C_5H_8} + \mathrm{HO_2} \leftrightarrow c\mathrm{C_5H_7} + \mathrm{H_2O_2}$	1.60E+11	0.0	17060
R6	$c\mathrm{C_5H_8} + \mathrm{O_2} \leftrightarrow c\mathrm{C_5H_7} + \mathrm{HO_2}$	1.28E+10	0.0	25000
R7	$c\mathrm{C_5H_7} + \mathrm{OH} \leftrightarrow c\mathrm{C_5H_6} + \mathrm{H_2O}$	6.02E+12	0.0	0.0
R8	$c\mathrm{C_5H_7} + \mathrm{O} \leftrightarrow c\mathrm{C_5H_6} + \mathrm{OH}$	1.80E+13	0.0	0.0
R9	$c\mathrm{C_5H_7} + \mathrm{H} \leftrightarrow c\mathrm{C_5H_6} + \mathrm{H_2}$	3.16E+13	0.0	13353
R10	$c\mathrm{C_5H_7} + \mathrm{HO_2} \leftrightarrow c\mathrm{C_5H_6} + \mathrm{H_2O_2}$	2.65E+12	0.0	0.0
R11	$c\mathrm{C_5H_7} + \mathrm{O_2} \leftrightarrow c\mathrm{C_5H_6} + \mathrm{HO_2}$	1.01E+12	0.0	13353

Note. Rate coefficient k is given by $k = AT^n\exp(-E_a/T)$. Units are $\mathrm{cm^3}$, s, K.

Table 2

Compounds in the mass spectrum in Fig. 7; ionization energies (IE) are taken from [55]

Number of C atoms	Aromatic compounds	Formula	*m/z*	IE (eV)
C_6	Benzene	A1 or C_6H_6	78	9.24
C_7	Toluene	C_7H_8	92	8.82
	Phenol[a]	C_6H_5OH	94	8.51
C_8	Phenylacetylene	$A1C_2H$ or C_8H_6	102	8.82
	Styrene	$A1C_2H_3$ or C_8H_8	104	8.43
C_9	Indene	A2R5 or C_9H_8	116	8.14
C_{10}	Naphthalene	A2 or $C_{10}H_8$	128	8.14
C_{11}	Methylnaphthalene	$C_{11}H_{10}$	142	7.96/7.83[b]
C_{12}	Acenaphthylene	$C_{12}H_8$	152	8.22
	Ethynylnaphthalene	$C_{12}H_8$	152	8.03/8.11[b]
	Biphenyl	$C_{12}H_{10}$	154	8.27
	Acenaphthene	$C_{12}H_{10}$	154	7.75
	Ethenylnaphthalene	$C_{12}H_{10}$	154	7.70
C_{13}	Benzindene	$C_{13}H_{10}$	166	no data found
	Fluorene	$C_{13}H_{10}$	166	7.89
	Methylacenaphthylene	$C_{13}H_{10}$	166	no data found
C_{14}	Phenanthrene	A3 or $C_{14}H_{10}$	178	7.89
	Anthracene	A3L or $C_{14}H_{10}$	178	7.46
C_{16}	Pyrene	A4 or $C_{16}H_{10}$	202	7.43
	Fluoranthene	A4 or $C_{16}H_{10}$	202	7.95

[a] Because of its mass, phenol is grouped with toluene although it features only six carbon atoms.

[b] The first value represents the 1-isomer, the second one the 2-isomer.

Table 3

Maximum signal intensity in the cyclopentene flame vs maximum signal intensity in the propene flame, $I_{cyclopentene}/I_{propene}$, for different masses

m/z	$I_{cyclopentene}/I_{propene}$		
	Experiment	Simulation	
		DLR model	MIT model
78	3.5± 0.4	0.82	3.4
92	3.2	0.89	14
94	3.9	1.3	2.0
102	5.3	8.1	370
104	4.5	2.7	8.4
116	6.5	190	2900
128	6.9	320	17000
142	4.3	100	1 me naph: 1700
			2 me naph: 4400
			sum: 3700
152	3.1	ethy naph: 190	1 ethy naph: 24000
			2 ethy naph: 22000
		acenaphthylene: 210	acenaphthylene: 1400
		sum: 200	**sum:** 5300
154	5.2	biphenyl: 1.5	biphenyl: 18
			ethe naph: 2200
			acenaphthene: 200
			sum: 630
166	6.1	me acenaphthylene: 150	
		fluorene: 1.0	
		sum: 130	
178	5.0	phen: 1500	phen: 44000

	anthr: 1300	anthr: 43000
	sum: 1400	**sum:** 44000
202	1.8	

Note. Assignment to structures can be found in Table 2; me = methyl, naph = naphthalene, ethy = ethynyl, ethe = ethenyl, phen = phenanthrene, anthr = anthracene.

Table 4

Arrhenius expressions for reaction (R23): $2C_3H_3 \rightarrow$ A1 (benzene)

A	n	E_a	Reference
6.00E+12	0.0	0	Scherer et al. [43]
3.00E+12	0.0	0	Richter and Howard [37]
3.49E+11	0.0	−3534	Fernandes et al. [58]

Note. Rate coefficient k is given by $k = AT^n \exp(-E_a/T)$. Units are cm^3, s, K.

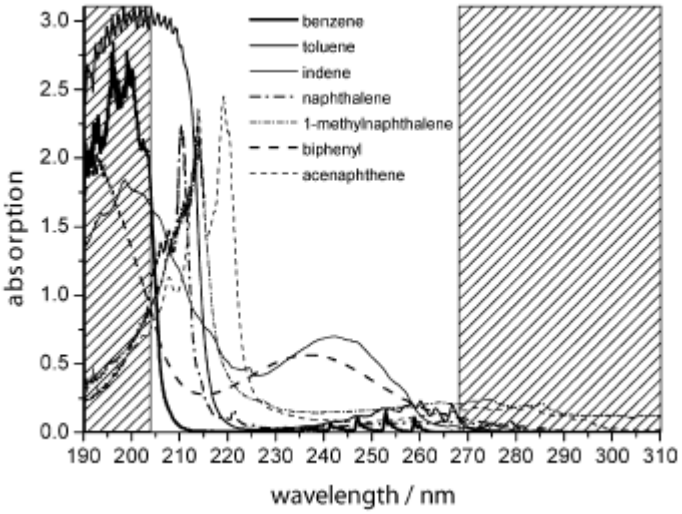

Fig. 1. UV absorption spectra of some relevant aromatic species.

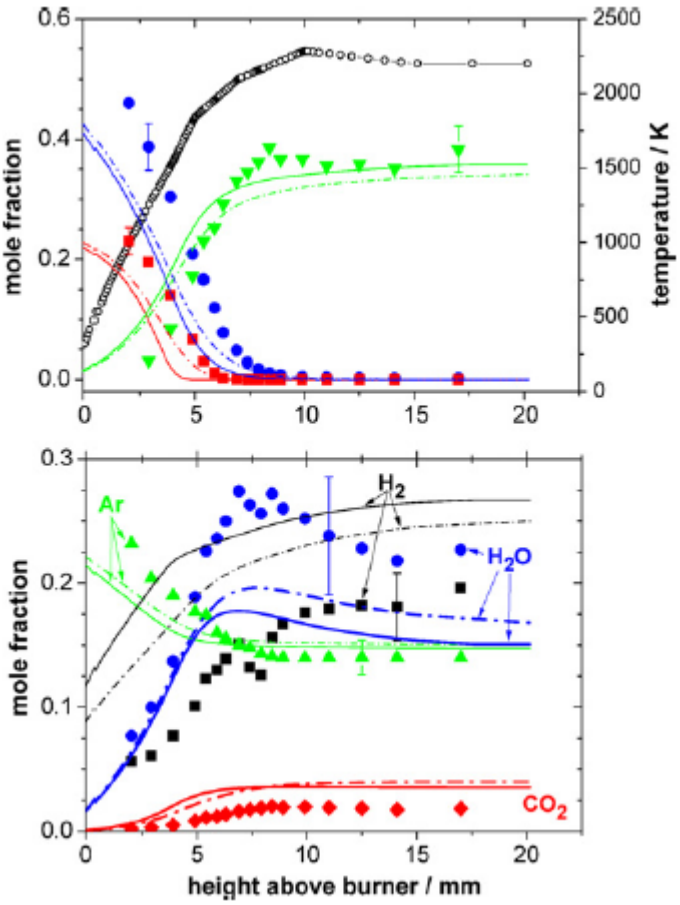

Fig. 2. Propene flame, major species mole fractions. Solid lines: DLR mechanism; broken lines:MIT mechanism; symbols: EI-MBMS experiment. Top: temperature (open circles, right axis), fuel (squares), O_2 (filled circles), and CO (triangles). Bottom: argon (triangles), H_2 (squares), H_2O (circles), and CO_2 (diamonds).

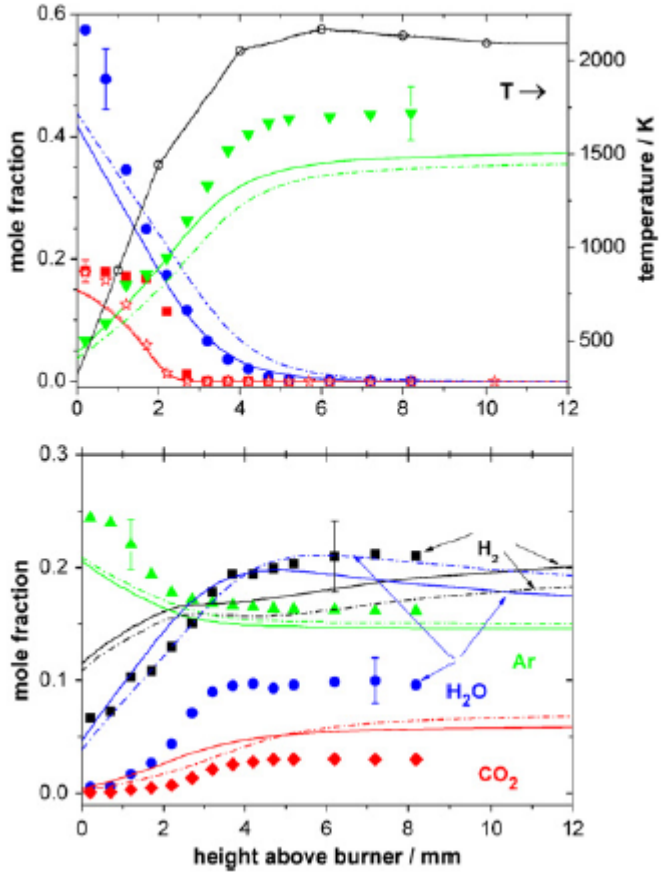

Fig. 3. Cyclopentene flame, major species mole fractions. Solid lines: DLR mechanism; broken lines: MIT mechanism; symbols: EI-MBMS experiment. Top: temperature (open circles, right axis), fuel (squares and stars), O_2 (filled circles), and CO (triangles). Bottom: argon (triangles), H_2 (squares), H_2O (circles), and CO_2 (diamonds).

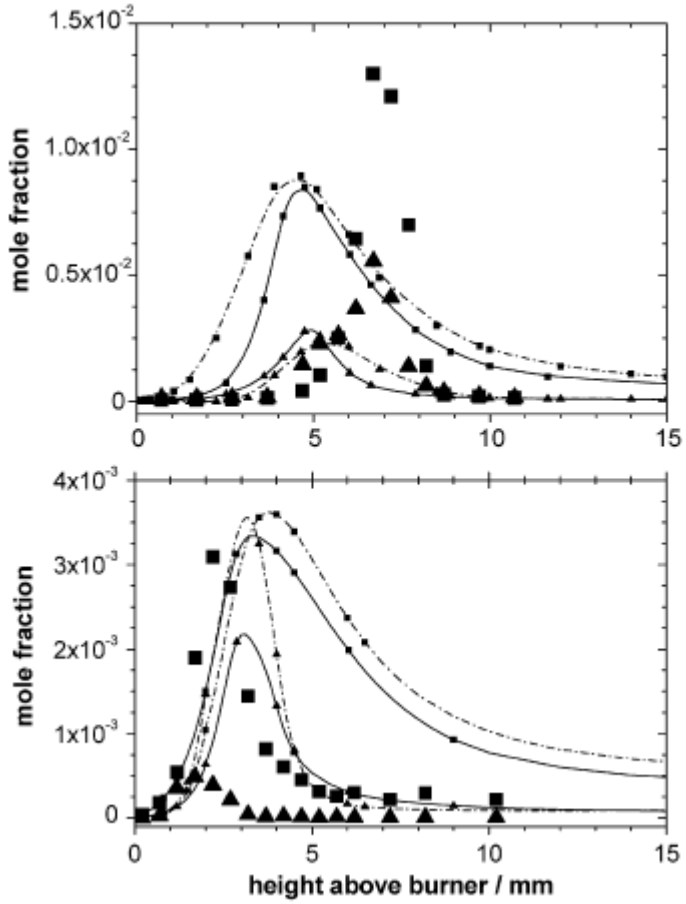

Fig. 4. Methyl (CH_3, squares) and propargyl (C_3H_3, H_2CCCH, triangles) mole fractions. Solid lines: DLR mechanism; broken lines: MIT mechanism; symbols: EI-MBMS experiment. Top: propene flame; bottom: cyclopentene flame.

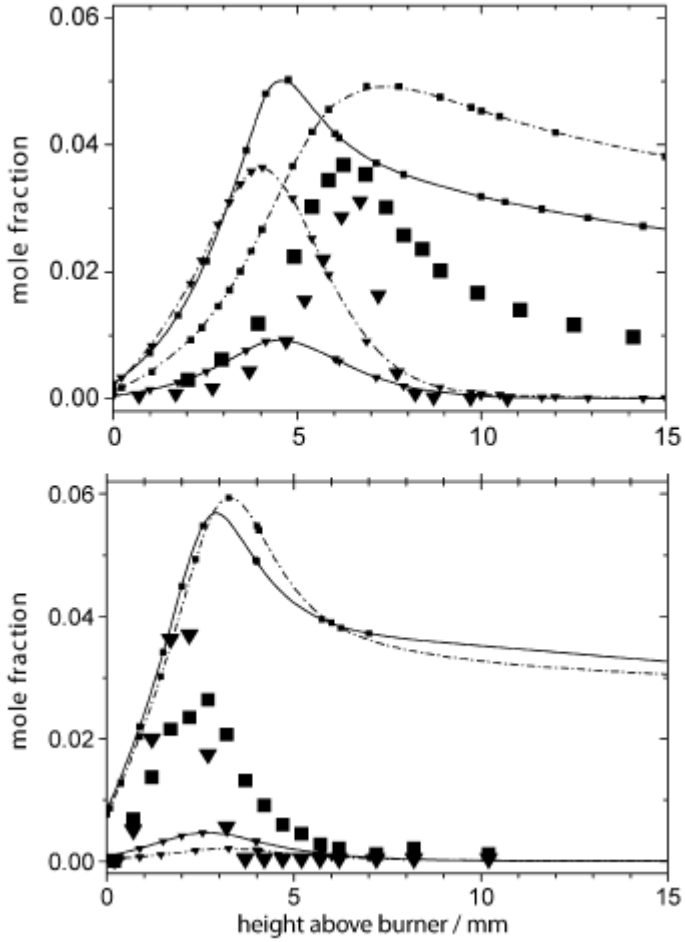

Fig. 5. Acetylene (C_2H_2, squares) and ethene (C_2H_4, triangles) mole fractions. Solid lines: DLR mechanism; broken lines: MIT mechanism; symbols: EI-MBMS experiment. Top: propene flame; bottom: cyclopentene flame.

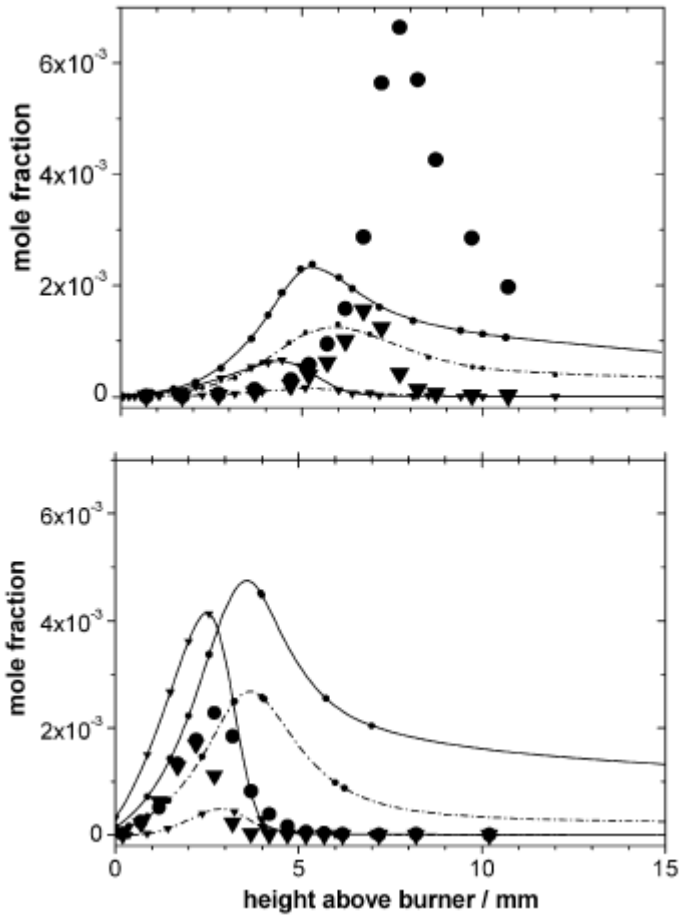

Fig. 6. Diacetylene (C_4H_2, circles) and vinylacetylene (C_4H_4, triangles) mole fractions. Solid lines: DLR mechanism; broken lines: MIT mechanism; symbols: EI-MBMS experiment. Top: propene flame; bottom: cyclopentene flame.

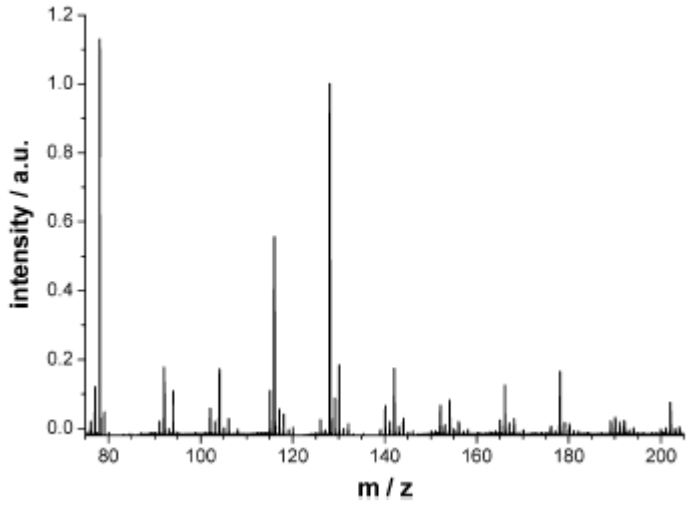

Fig. 7. Mass spectrum taken in the cyclopentene flame at 255 nm and HAB 2.7 mm.

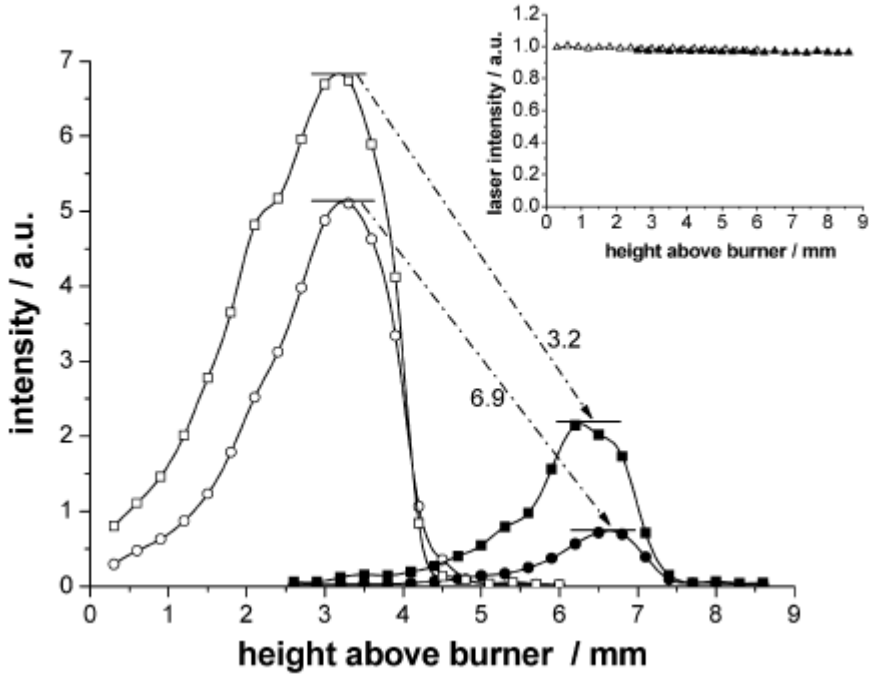

Fig. 8. REMPI-MBMS signal intensities at *m/z* = 92 (toluene, squares) and *m/z* = 128 (naphthalene, circles) in propene flame (filled symbols) and cyclopentene flame (open symbols); the intensity ratio $I_{cyclopentene}/I_{propene}$ is 3.2 at *m/z* = 92 and 6.9 at *m/z* = 128 (arrows), respectively. The inset shows the laser intensity for both measurements.

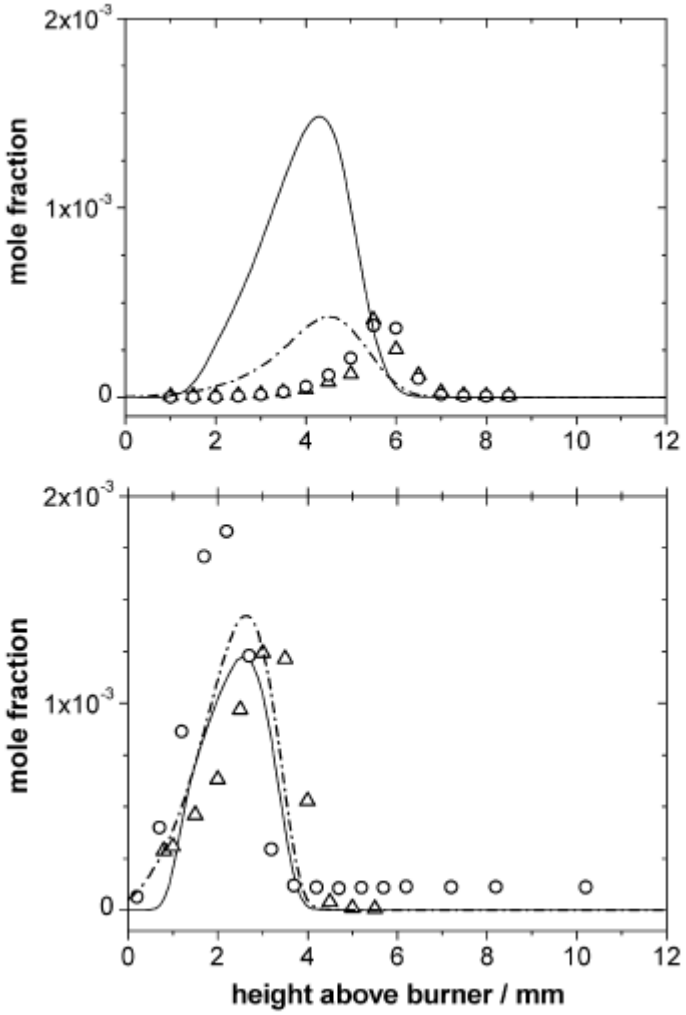

Fig. 9. Benzene (A1, C_6H_6) mole fraction. Solid lines: DLR mechanism; broken lines: MIT mechanism; circles: EI-MBMS, triangles: REMPI-MBMS experiment. Top: propene flame; bottom: cyclopentene flame.

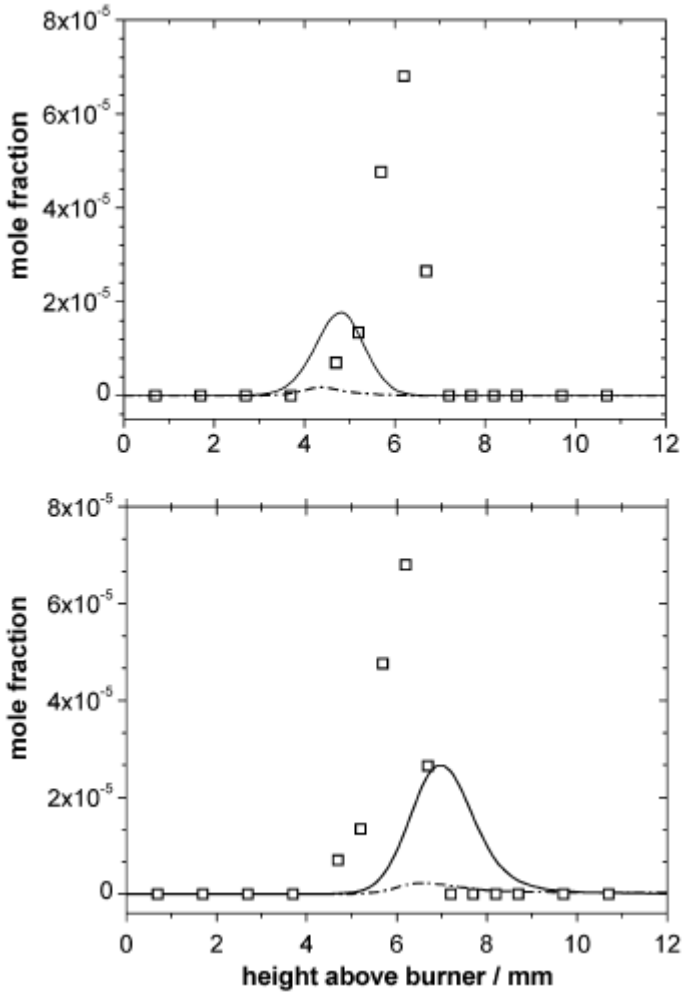

Fig. 10. Phenyl (A1–, C_6H_5) mole fraction. Solid lines: DLR mechanism; broken lines: MIT mechanism; squares: EI-MBMS experiment. Top: propene flame; bottom: cyclopentene flame.

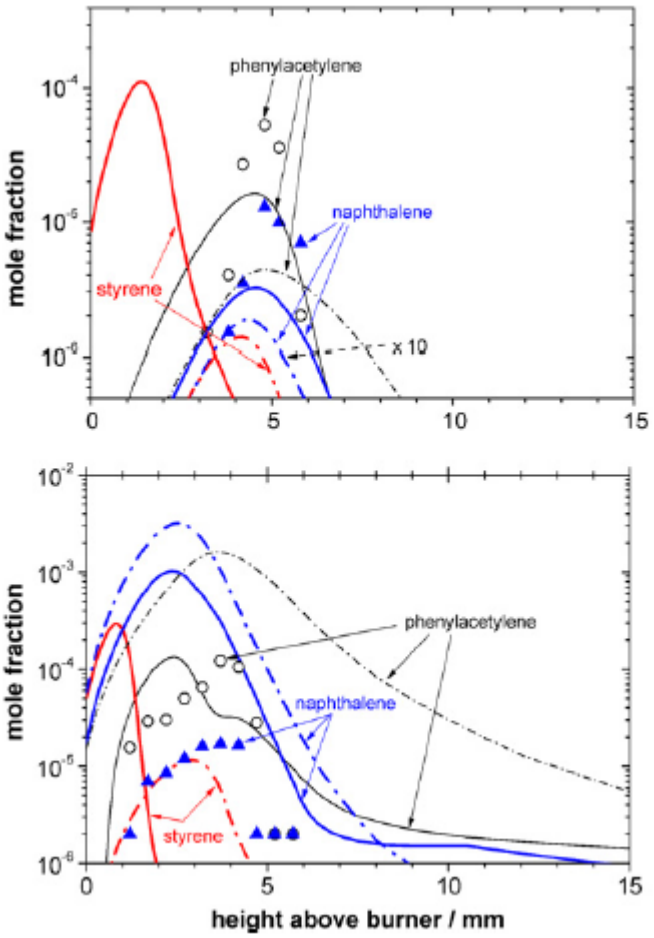

Fig. 11. Phenylacetylene (A1C_2H, C_8H_6, circles), styrene (A1C_2H_3, C_8H_8) and naphthalene (A2, $C_{10}H_8$, triangles) mole fractions. Solid lines: DLR mechanism; broken lines: MIT mechanism; symbols: EI-MBMS experiment. Top: propene flame; bottom: cyclopentene flame.

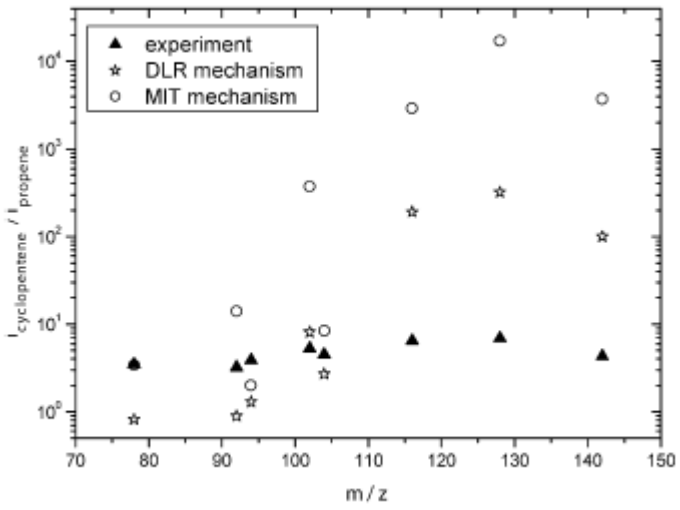

Fig. 12. Intensity ratio $I_{cyclopentene}/I_{propene}$ for several aromatic species (compare Tables 2 and 3 for structures and numerical values; note logarithmic scale).

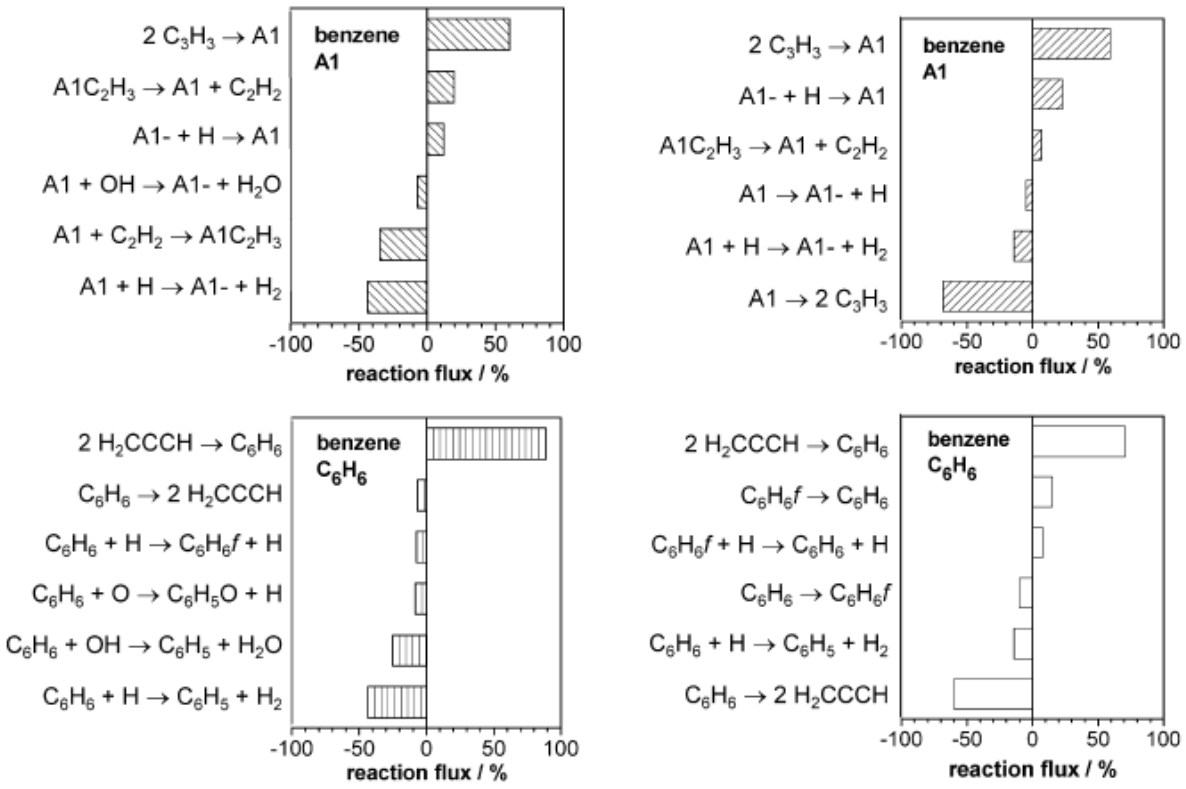

Fig. 13. Reaction flux analysis for benzene (A1, C_6H_6). Left: propene flame (HAB 4.5 mm); right: cyclopentene flame (HAB 3.5 mm). Top: DLR mechanism; bottom: MIT mechanism.

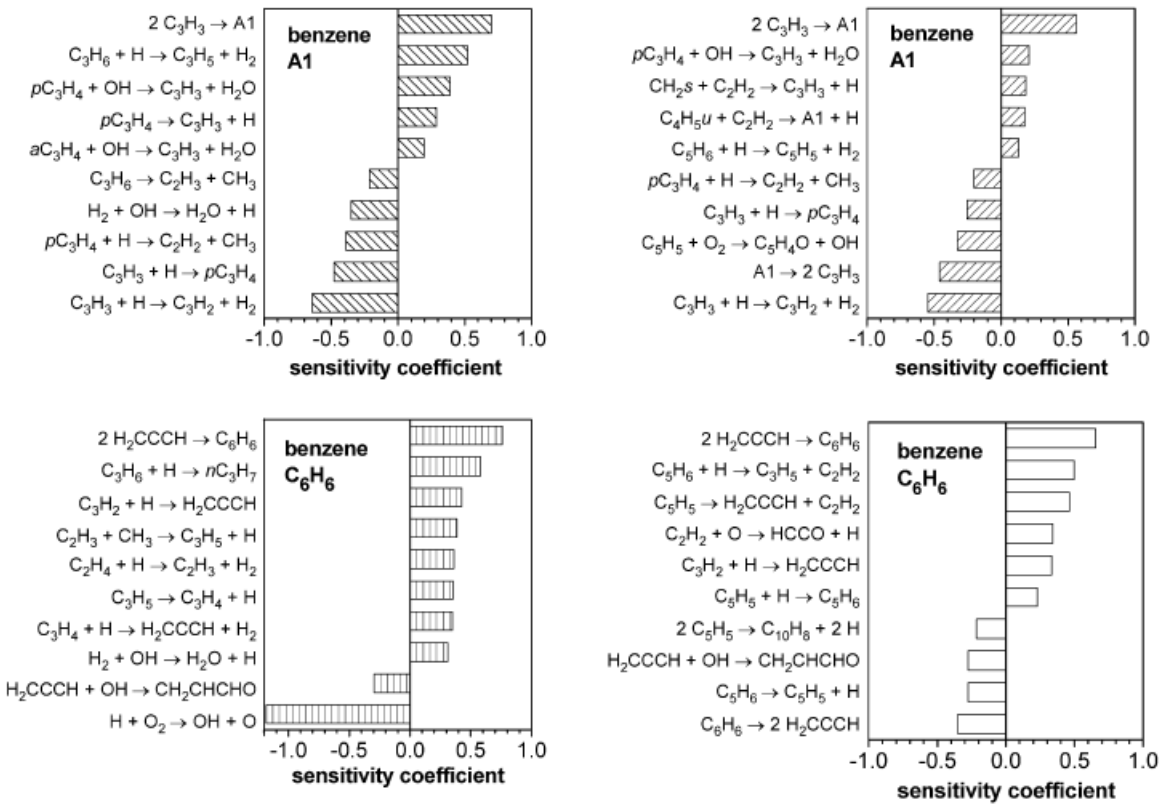

Fig. 14. Sensitivity analysis for benzene (A1, C_6H_6). Left: propene flame (HAB 4.5 mm); right: cyclopentene flame (HAB 3.5 mm). Top: DLR mechanism; bottom: MIT mechanism.

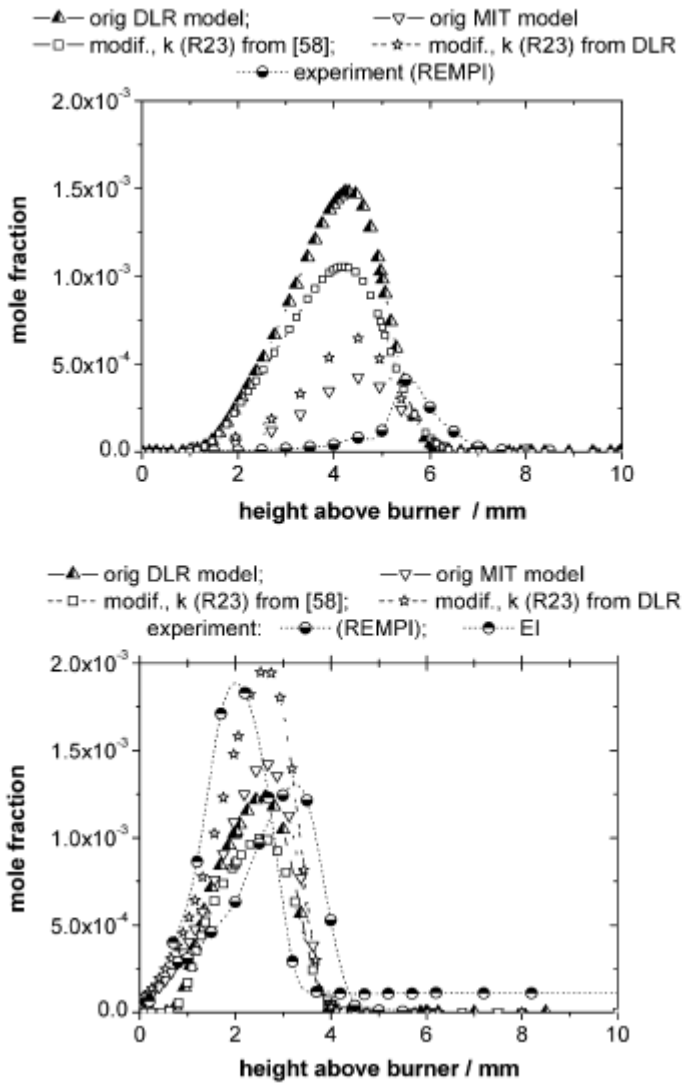

Fig. 15. Benzene (A1, C_6H_6) mole fraction; influence of the recombination reaction of propargyl radicals (R23). Filled triangles: original DLR mechanism; open triangles: MIT mechanism; semi-filled circles: EI-MBMS; filled circles: REMPI-MBMS experiment. Top: propene flame; bottom: cyclopentene flame.

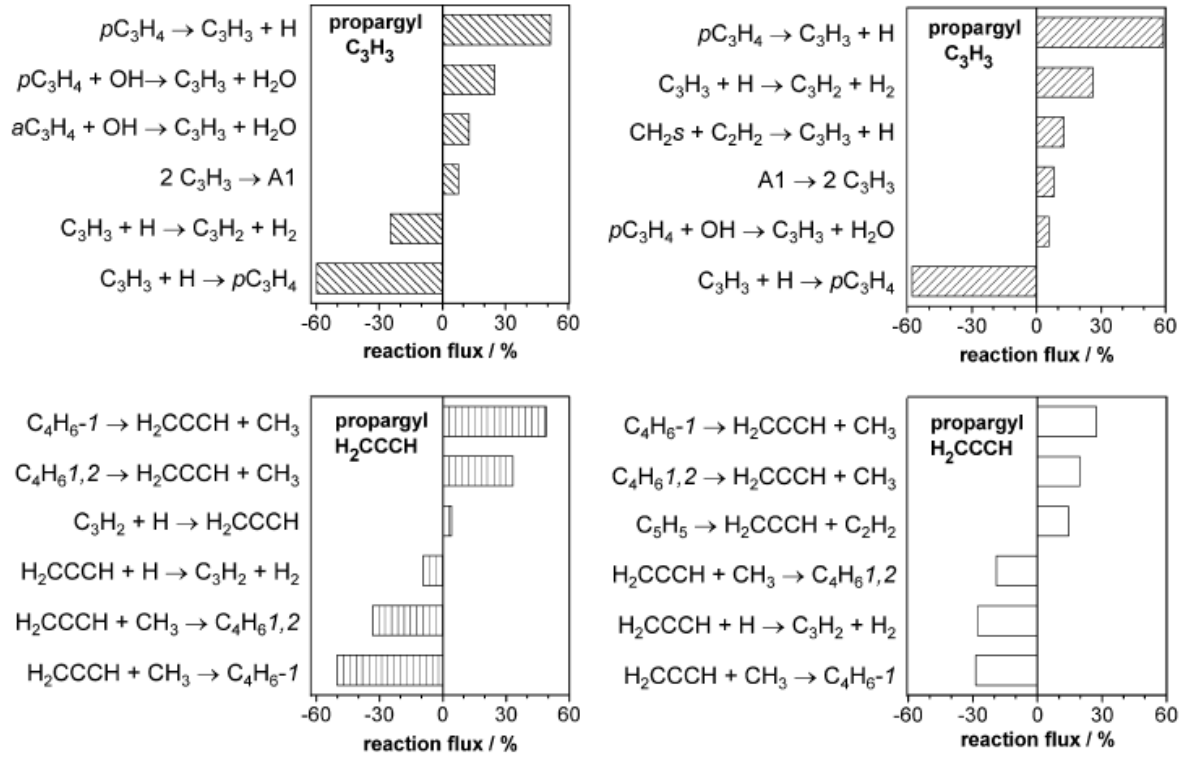

Fig. 16. Reaction flux analysis for propargyl (C_3H_3, H_2CCCH). Left: propene flame (HAB 4.5 mm); right: cyclopentene flame (HAB 3.5 mm). Top: DLR mechanism; bottom: MIT mechanism.

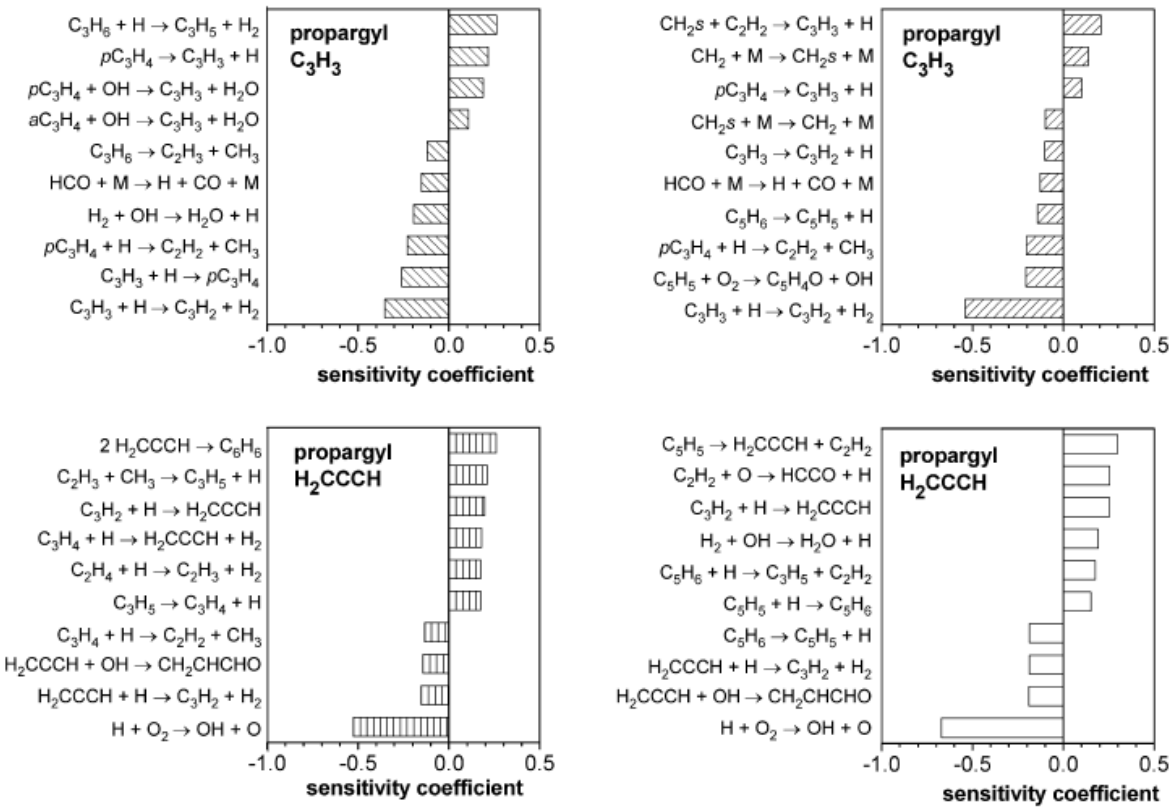

Fig. 17. Sensitivity analysis for propargyl (C_3H_3, H_2CCCH). Left: propene flame (HAB 4.5 mm); right: cyclopentene flame (HAB 3.5 mm). Top: DLR mechanism; bottom: MIT mechanism.

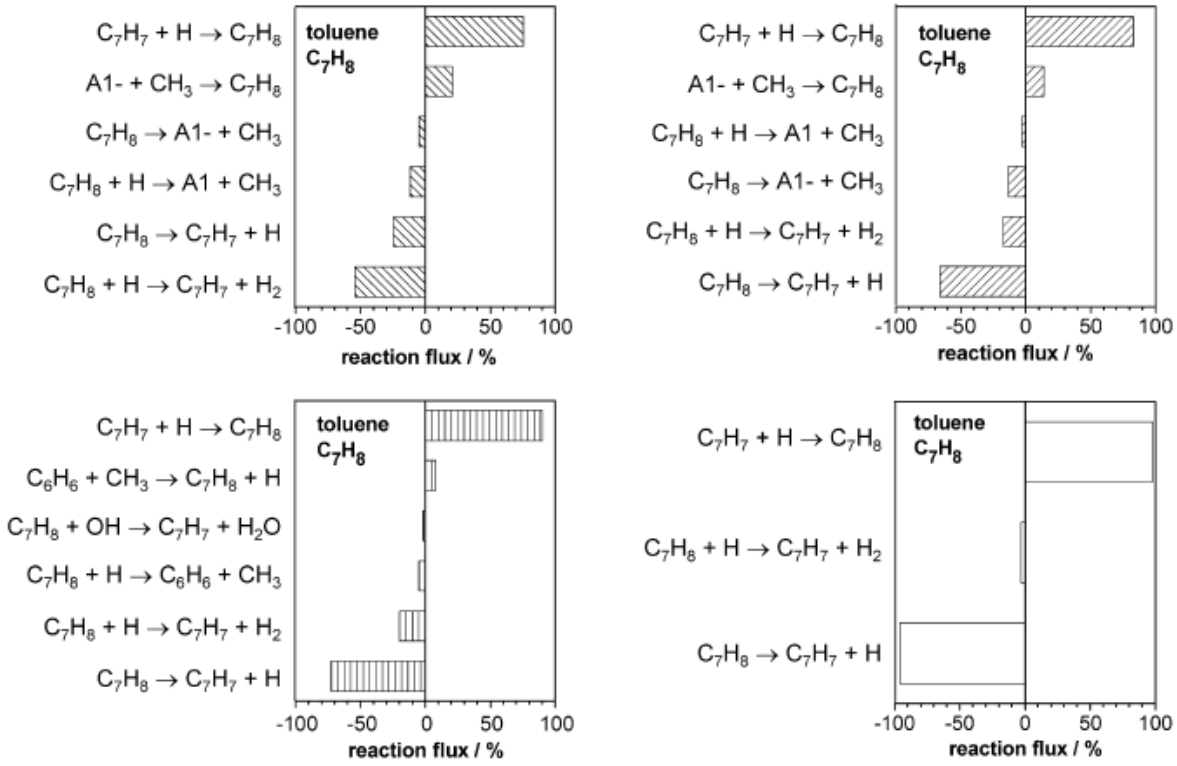

Fig. 18. Reaction flux analysis for toluene (C_7H_8). Left: propene flame (HAB 4.5 mm); right: cyclopentene flame (HAB 3.5 mm). Top: DLR mechanism; bottom: MIT mechanism.

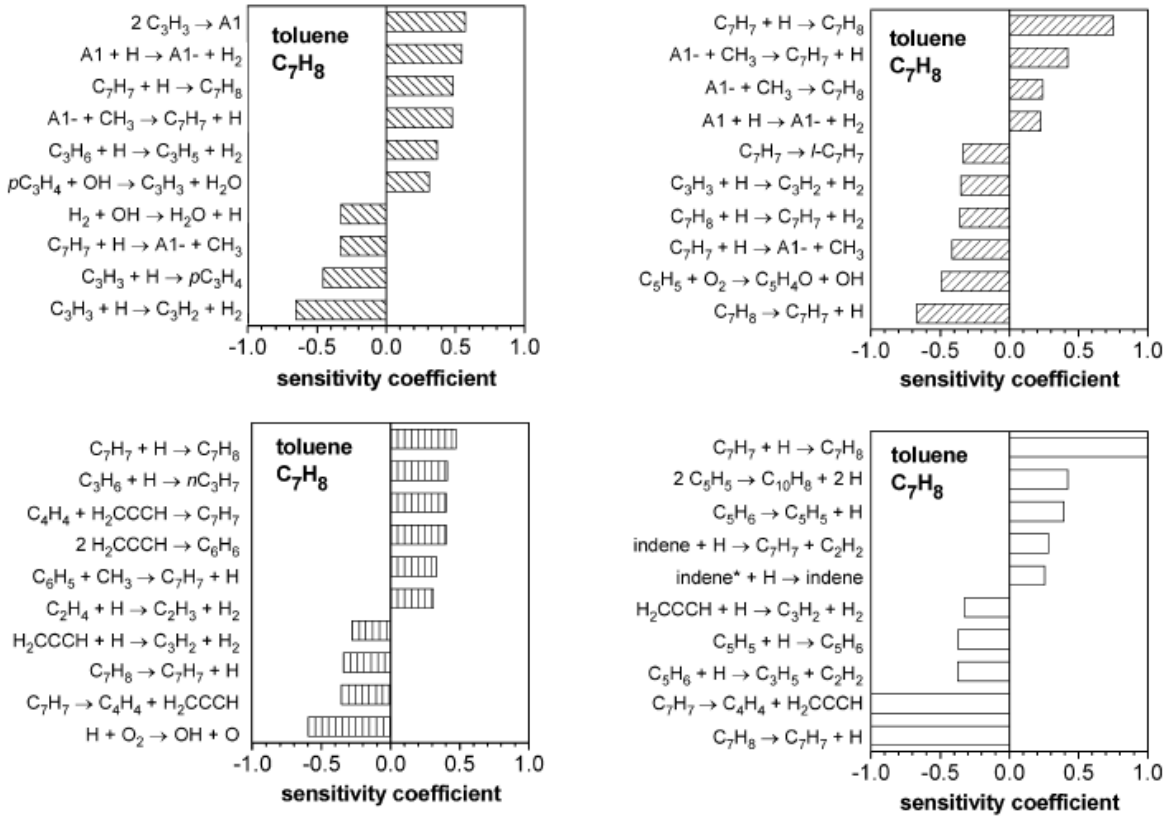

Fig. 19. Sensitivity analysis for toluene (C_7H_8). Left: propene flame (HAB 4.5 mm); right: cyclopentene flame (HAB 3.5 mm). Top: DLR mechanism; bottom: MIT mechanism.

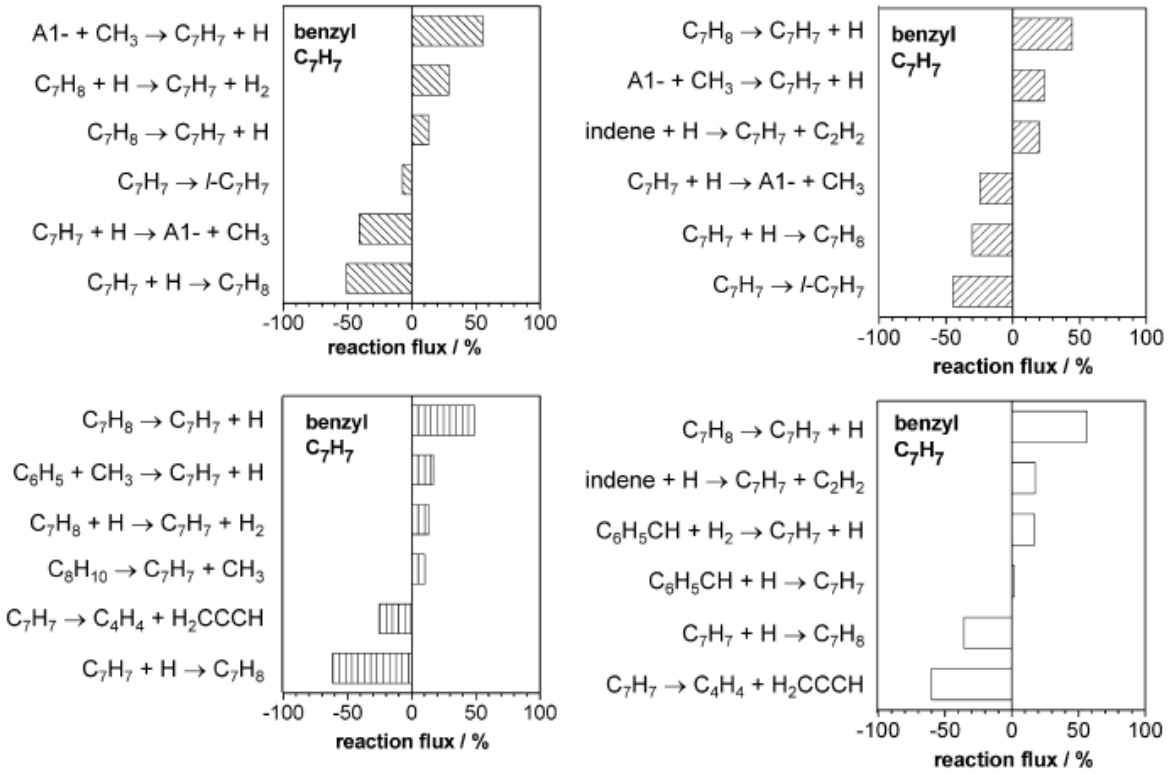

Fig. 20. Reaction flux analysis for benzyl (C_7H_7). Left: propene flame (HAB 4.5 mm); right: cyclopentene flame (HAB 3.5 mm). Top: DLR mechanism; bottom: MIT mechanism.

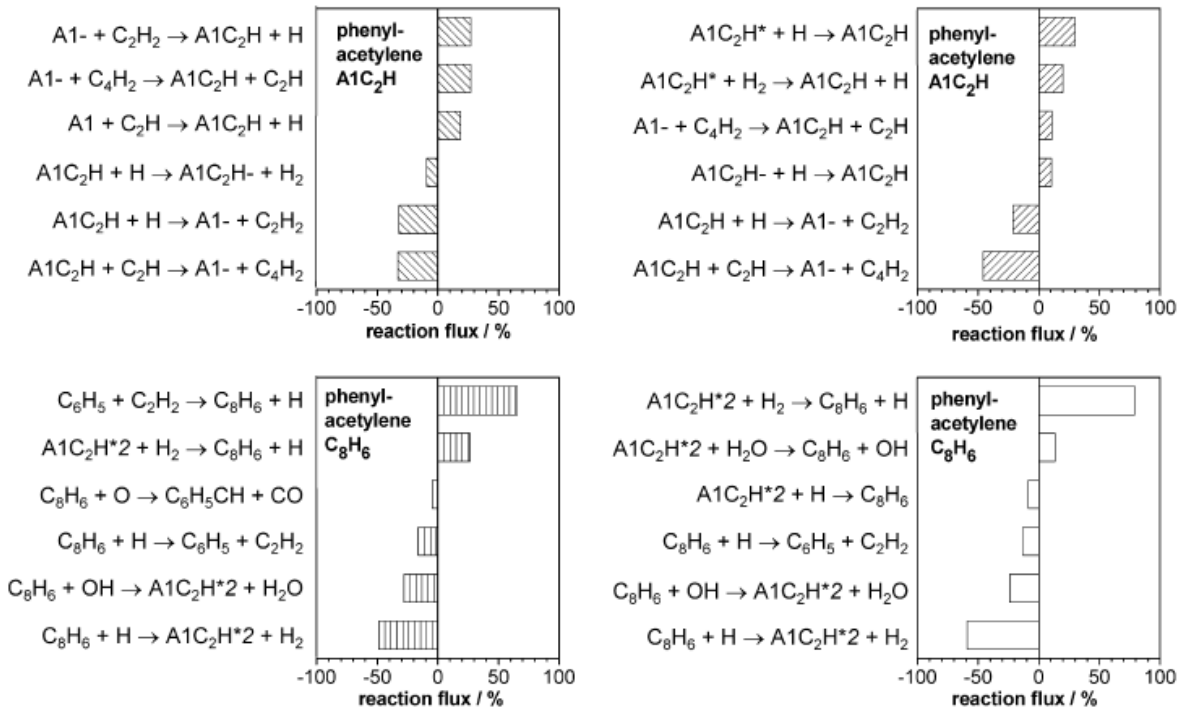

Fig. 21. Reaction flux analysis for phenylacetylene ($A1C_2H$, C_8H_6) Left: propene flame (HAB 4.5 mm); right: cyclopentene flame (HAB 3.5 mm). Top: DLR mechanism; bottom: MIT mechanism.

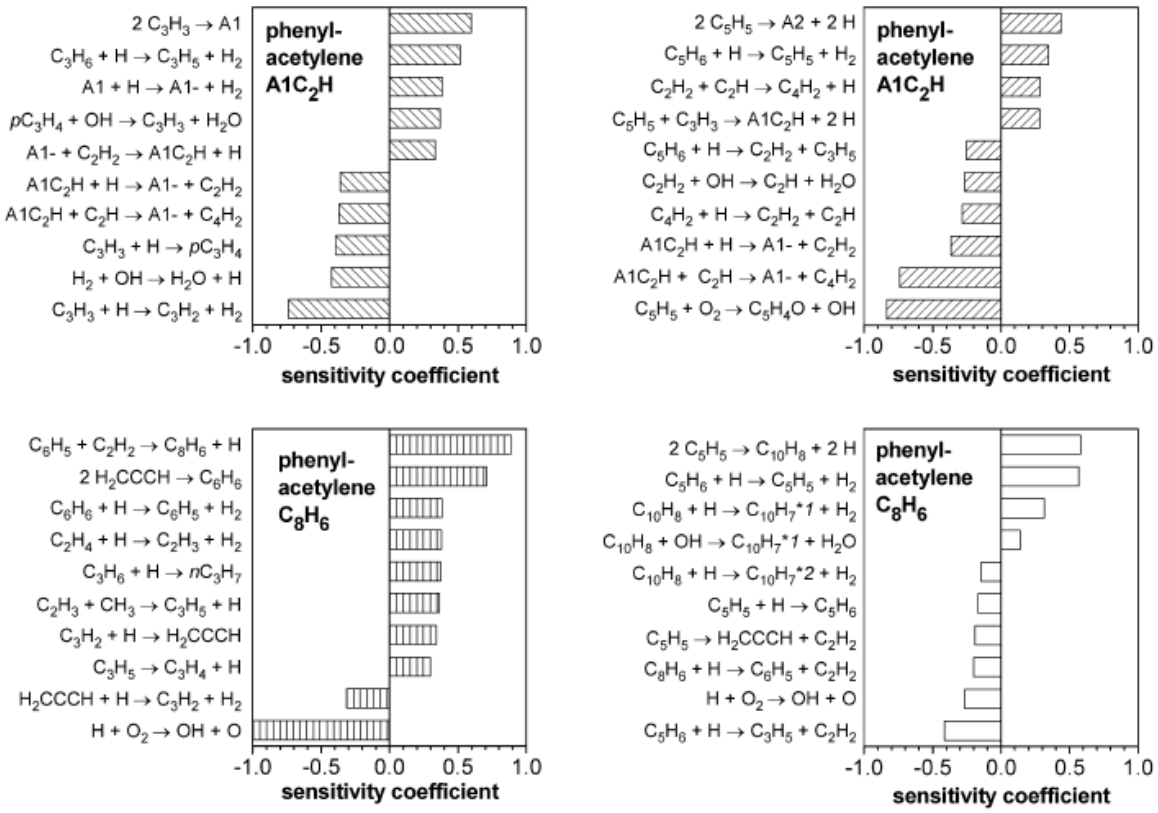

Fig. 22. Sensitivity analysis for phenylacetylene ($A1C_2H$, C_8H_6) Left: propene flame (HAB 4.5 mm); right: cyclopentene flame (HAB 3.5 mm). Top: DLR mechanism; bottom: MIT mechanism.

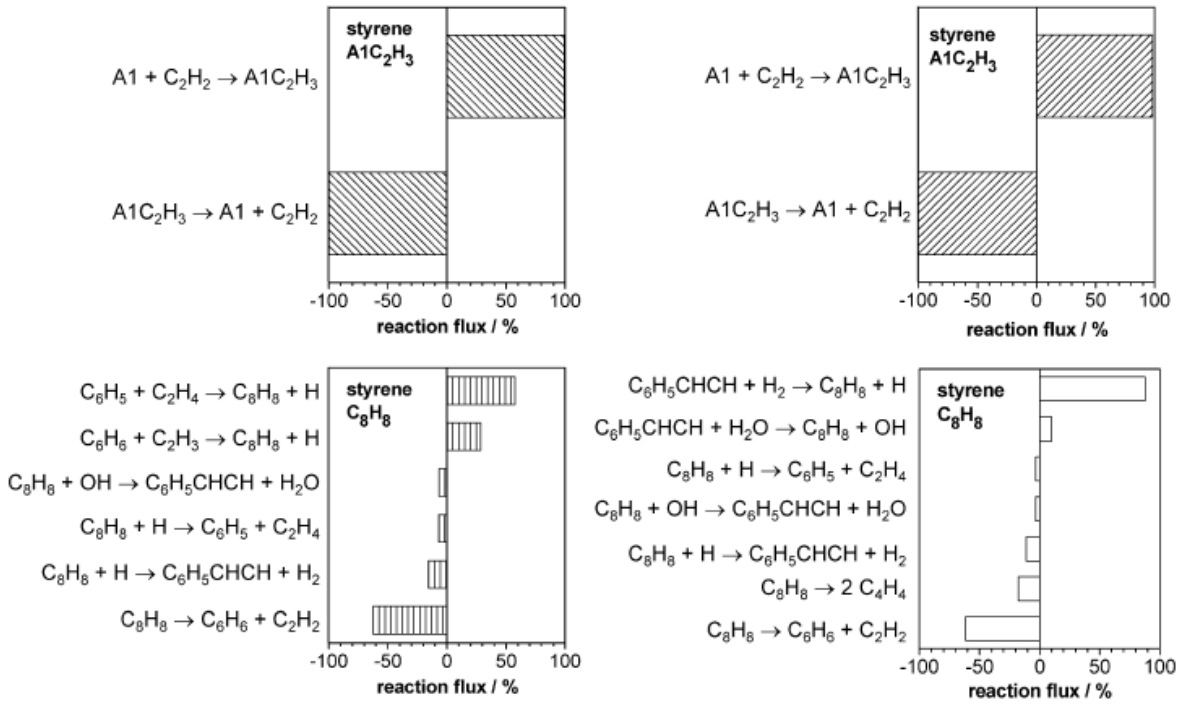

Fig. 23. Reaction flux analysis for styrene ($A1C_2H_3$, C_8H_8). Left: propene flame (HAB 4.5 mm); right: cyclopentene flame (HAB 3.5 mm). Top: DLR mechanism; bottom: MIT mechanism.

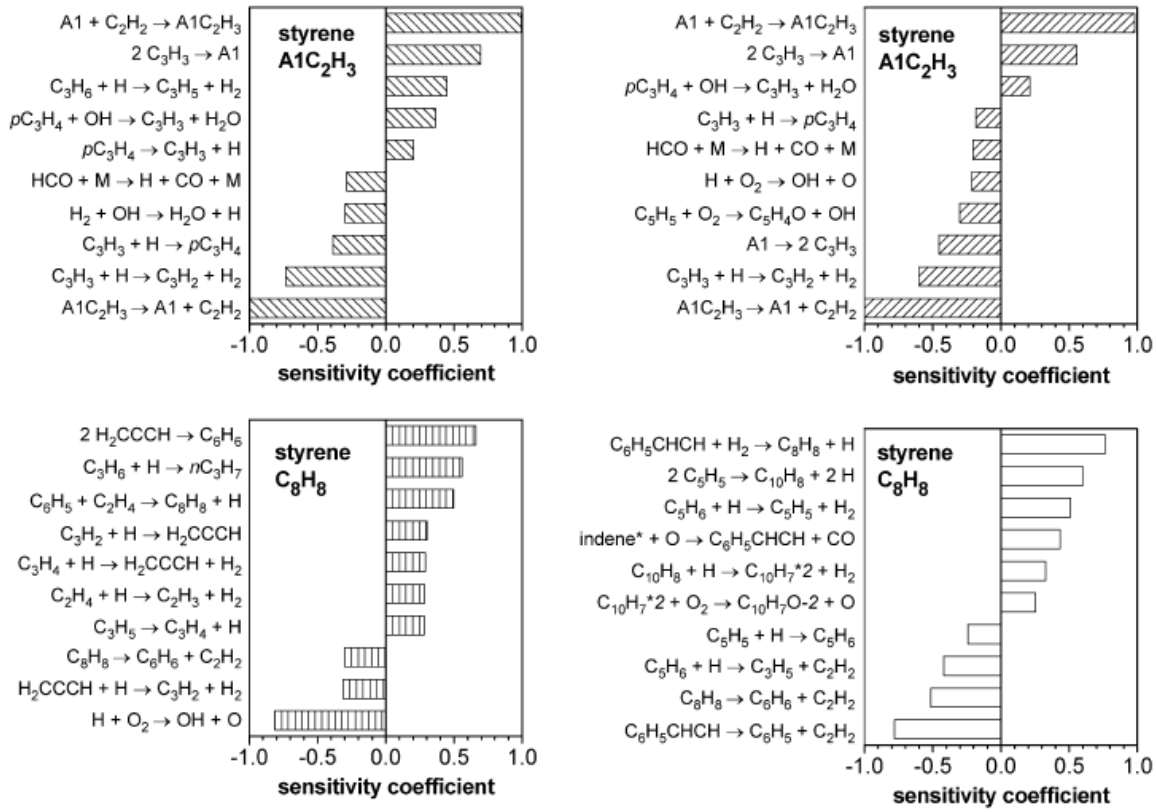

Fig. 24. Sensitivity analysis for styrene ($A1C_2H_3$, C_8H_8). Left: propene flame (HAB 4.5 mm); right: cyclopentene flame (HAB 3.5 mm). Top: DLR mechanism; bottom: MIT mechanism.

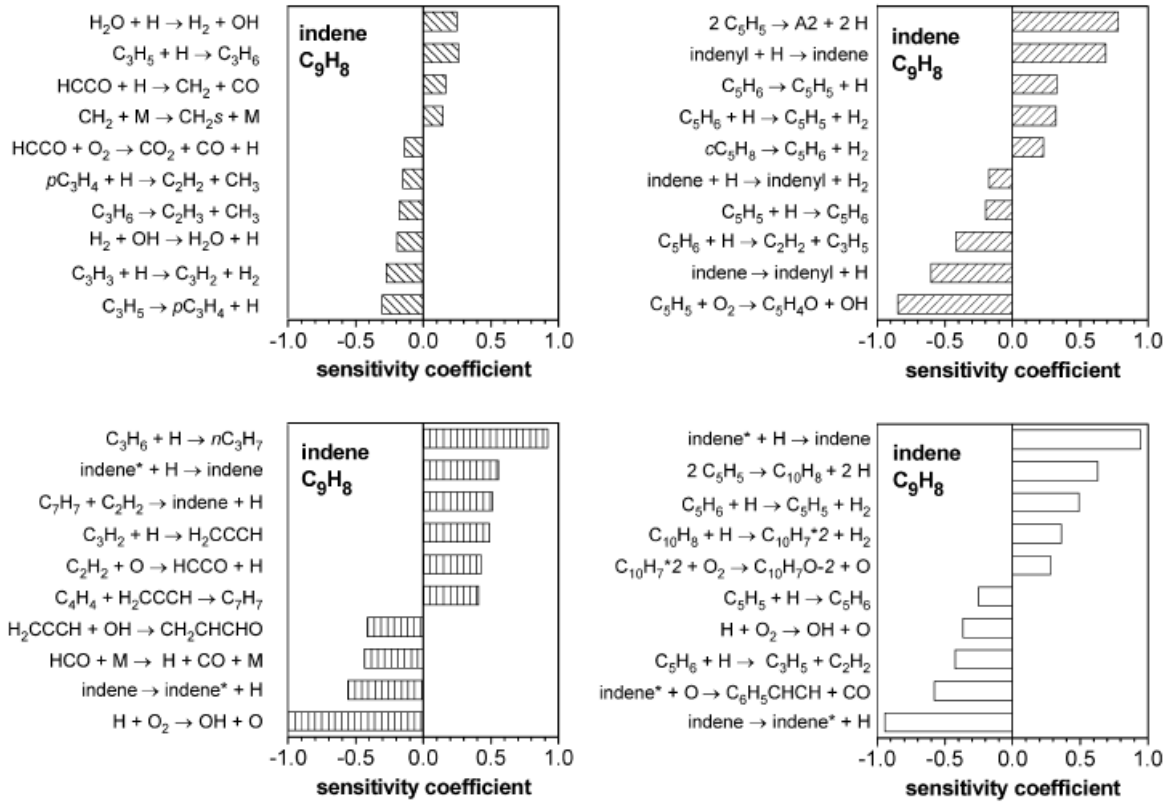

Fig. 25. Sensitivity analysis for indene (C_9H_8). Left: propene flame (HAB 4.5 mm); right: cyclopentene flame (HAB 3.5 mm). Top: DLR mechanism; bottom: MIT mechanism.

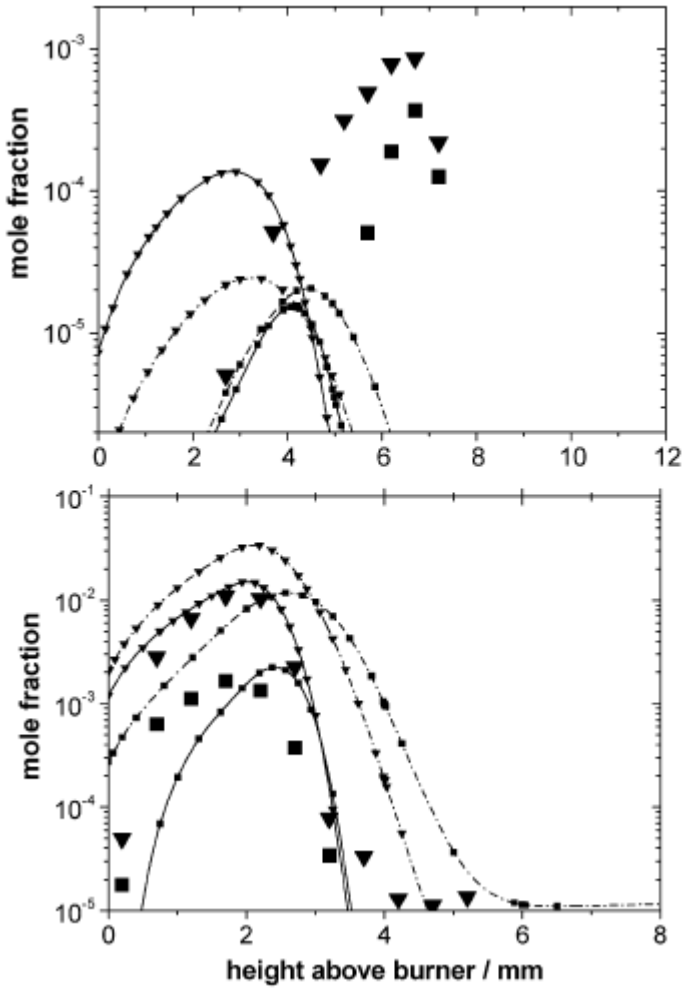

Fig. 26. Cyclopentadienyl ($c$$C_5H_5$, squares) and cyclopentadiene ($c$$C_5H_6$, triangles) mole fractions. Solid lines: DLR mechanism; broken lines: MIT mechanism; symbols: EI-MBMS experiment. Top: propene flame; bottom: cyclopentene flame.

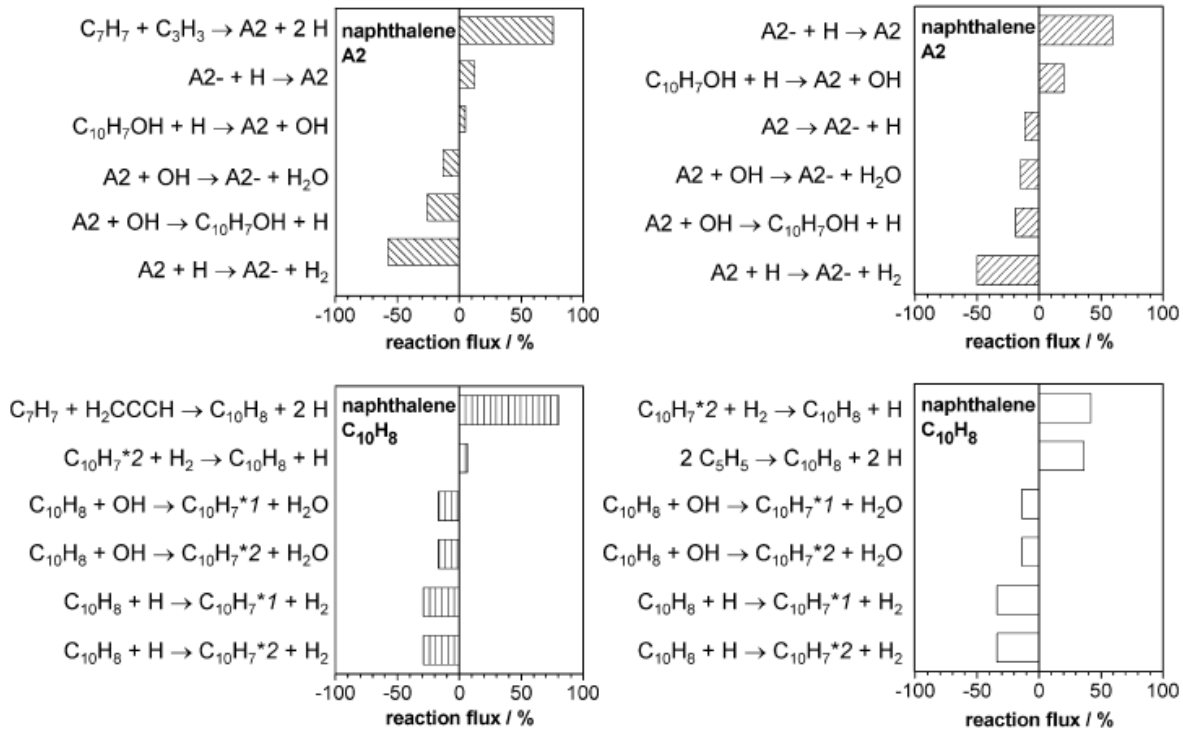

Fig. 27. Reaction flux analysis for naphthalene (A2, $C_{10}H_8$). Left: propene flame (HAB 4.5 mm); right: cyclopentene flame (HAB 3.5 mm). Top: DLR mechanism; bottom: MIT mechanism.

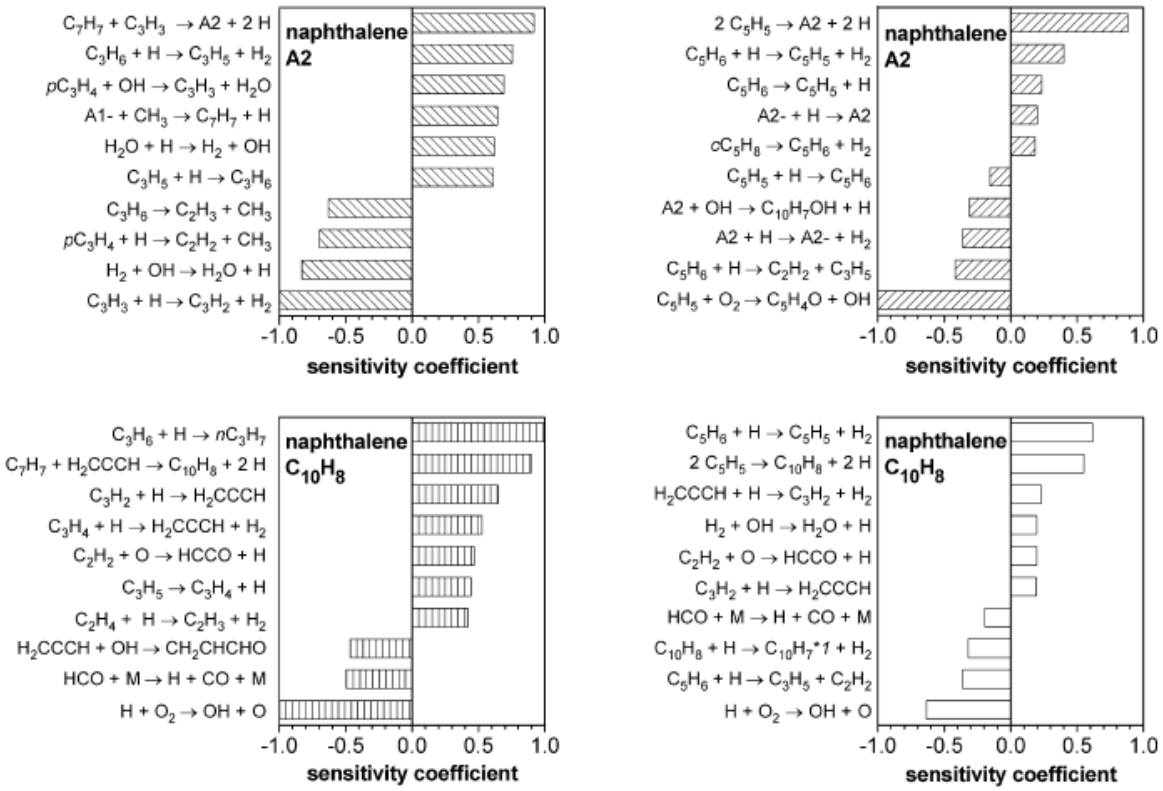

Fig. 28. Sensitivity analysis for naphthalene (A2, $C_{10}H_8$). Left: propene flame (HAB 4.5 mm); right: cyclopentene flame (HAB 3.5 mm). Top: DLR mechanism; bottom: MIT mechanism.